ORNL/TM-2023/2834

Transition Core Modeling for Extended Enrichment & Accident-Tolerant Fuels Using Polaris/PARCS

Steve E. Skutnik
Ugur Mertyurek
Muhammad Rizki Oktavian
William A. Wieselquist

July 2023

OAK RIDGE National Laboratory

ORNL IS MANAGED BY UT–BATTELLE, LLC, FOR THE U.S. DEPARTMENT OF ENERGY

ORNL/TM-2023/2834

Nuclear Energy & Fuel Cycle Division

TRANSITION CORE MODELING FOR EXTENDED ENRICHMENT & ACCIDENT-TOLERANT FUELS USING POLARIS/PARCS

Steve E. Skutnik
Ugur Mertyurek
Muhammad Rizki Oktavian
William A. Wieselquist

Date Published: July 2023

Prepared by
OAK RIDGE NATIONAL LABORATORY
Oak Ridge, TN 37831-6283
managed by
UT-Battelle, LLC
for the
US DEPARTMENT OF ENERGY
under contract DE-AC05-00OR22725

CONTENTS

LIST OF FIGURES . . . . . **iv**
LIST OF TABLES . . . . . **vii**
ACRONYMS . . . . . **ix**
EXECUTIVE SUMMARY . . . . . **x**
ACKNOWLEDGMENTS . . . . . **xii**
1. INTRODUCTION **1**
2. ASSEMBLY MODELS **3**
   2.1 Polaris PWR Assembly Model 3
   2.2 Polaris BWR Assembly Model 4
3. PWR MULTI-ASSEMBLY CALCULATION **8**
   3.1 PWR 3×3 Model 8
   3.2 Group Structure Comparison for All-Fresh Multi-Assembly Models 9
   3.3 LEU to LEU core 11
   3.4 LEU to LEU+ transition core 14
   3.5 LEU to ATF transition core 17
   3.6 Reactivity coefficients for the transition cores 17
4. BWR MULTI-ASSEMBLY CALCULATION **21**
   4.1 BWR 2×2 multi-assembly model 21
   4.2 Group structure comparison 21
      4.2.1 Nominal void condition 22
      4.2.2 High-void condition 24
   4.3 LEU-to-LEU transition core 26
   4.4 LEU-to-LEU+ transition core 27
   4.5 LEU-to-ATF core 31
   4.6 Reactivity analysis of the BWR multi-assembly transition cycles 33
5. BWR FULL-CORE TRANSITION CYCLE CALCULATION **36**
   5.1 Polaris/PARCS BWR Whole-Core Model 36
   5.2 Core Power Distributions 37
   5.3 Reactivity Coefficients and Control Blade Worth 39
6. CONCLUSIONS **41**
REFERENCES **43**
A. TESTING PROCEDURE FOR PIN POWERS IN A NON-UNIFORM LATTICE GEOMETRY . **A–1**
   A.1 Test problem A–2
   A.2 Test results A–3
   A.3 Test inputs A–3
      A.3.1 Polaris 56-group test input A–3
      A.3.2 TRITON/NEWT 56-group test input A–4

LIST OF FIGURES

1 Westinghouse PWR 17 × 17 quarter assembly, showing fuel pins (red) and coolant guide tube (blue). . . . 4
2 Pin enrichments and gadolinia concentration (wt. %) for the BWR LEU assemblies used for this study . . . 5
3 Pin enrichments and gadolinia concentration (wt. %) for the 8 w/o ^{235}U maximum enrichment LEU+/ATF BWR assemblies used for this study . . . 6
4 Pin enrichments and gadolinia concentration (wt. %) for the 10 w/o ^{235}U maximum enrichment LEU+/ATF BWR assemblies used for this study . . . 6

5 Multi-assembly PWR multi-assembly models used for group sensitivity study. Note that the Polaris model (left) employs quarter-core symmetry (reflective boundary conditions). . . . 8
6 PWR 3 × 3 assembly model (SE symmetry) relative pin power differences for the PWR all-fresh LEU + LEU+ assembly configuration as compared to Polaris for the PARCS few-group models and Serpent CE model. . . . 10
7 Serpent 3 × 3 PWR lattice relative fission power (red/orange) and thermal flux (blue) distribution with SE symmetry. . . . 12
8 Relative pin power distribution for Polaris and Polaris/PARCS vs. Polaris for the LEU-to-LEU transition cycle . . . 12
9 Relative pin power differences for Polaris/PARCS vs. Polaris for the PWR LEU-to-LEU transition cycle . . . 13
10 k_{eff} comparison for transition models for PWR 3 × 3 assembly model (LEU-to-LEU core) compared between Polaris and PARCS for each burnup step; cycles boundaries occur at 533 and 1065 EFPD, with the transition core reload at 1066 EFPD. Shaded regions indicate (light orange) nominal core loading and (light blue) twice-burned LEU assemblies surrounded by fresh LEU assemblies. . . . 14
11 Relative pin power distribution for Polaris and Polaris/PARCS vs. Polaris for the PWR LEU-to-LEU+ transition cycle . . . 15
12 Relative pin power differences for Polaris/PARCS vs. Polaris for the PWR LEU-to-LEU+ transition cycle. . . . 15
13 k_{eff} comparison for transition models for the PWR 3 × 3 assembly model (LEU-to-LEU+ core) compared between Polaris and PARCS for each burnup step; cycles boundaries occur at 533 and 1065 EFPD, with the transition core reload at 1066 EFPD. Shaded regions indicate (light orange) nominal core loading and (light blue) twice-burned LEU assemblies surrounded by LEU+ assemblies. . . . 16
14 Relative pin power distribution for Polaris and Polaris/PARCS vs. Polaris for the PWR LEU-to-ATF transition cycle. . . . 18
15 Relative pin power differences for Polaris/PARCS vs. Polaris for the PWR LEU-to-ATF transition cycle. . . . 18
16 k_{eff} comparison for transition models for the PWR 3×3 assembly model (LEU-to-ATF core) compared between Polaris and PARCS for each burnup step; cycles boundaries occur at 533 and 1065 EFPD, with the transition core reload at 1066 EFPD. Shaded regions indicate (light orange) nominal core loading and (light blue) twice-burned LEU assemblies surrounded by ATF assemblies. . . . 19
17 CRW at HFP for the 3 × 3 PWR assembly model in the third (transition) cycle. (Note that the LEU+ and ATF series values largely overlap.) . . . 19

18 DTC at HFP for the 3 × 3 PWR assembly model in the third (transition) cycle. 20

19 Multi-assembly BWR models used for group sensitivity study. 21
20 Relative pin power distribution for the Polaris model of the transition core multi-assembly model (LEU and LEU+ assemblies, all fresh) at nominal and high-void conditions. 22
21 Serpent BWR 2 × 2 lattice model and relative power distribution at the beginning of cycle for the LEU/LEU+ mixed core (all fresh assemblies). 23
22 Relative pin power differences (beginning of cycle) for the BWR 2 × 2 supercell for the LEU and LEU+ mixed core (all fresh assemblies) as compared to Polaris for the PARCS few-group models and Serpent CE model. 24
23 Relative pin power differences as compared to Polaris for the high-void transition cycle (LEU and LEU+ multi-assembly model, all fresh assemblies). 25
24 Relative pin power distribution calculated from Polaris for the LEU/LEU+ BWR transition core at BOC and EOC, wherein a twice-burned LEU assembly (NW) is surrounded by fresh LEU assemblies at 8.0 w/o ^{235}U (SE) and 10 w/o ^{235}U (SW and NE). 26
25 Relative pin power differences for Polaris/PARCS vs. Polaris for the BWR LEU-to-LEU transition cycle 27
26 Relative pin power distribution calculated from Polaris for the BWR transition core at BOC and EOC, wherein a twice-burned LEU assembly (NW) is surrounded by fresh LEU+ assemblies at 8 w/o ^{235}U (SE) and 10 w/o ^{235}U (SW and NE). 28
27 Relative pin power differences for Polaris/PARCS vs. Polaris for the BWR LEU-to-LEU+ transition cycle. 29
28 Pin enrichments and gadolinia concentration (wt. %) for the modified 10 w/o ^{235}U maximum enrichment LEU+ assembly used to isolate the cause of large observed pin power discrepancies at the assembly interfaces. 30
29 Relative pin power differences at BOC for Polaris/PARCS vs. Polaris for the BWR LEU-to-LEU+ transition cycle employing a modified LEU+ lattice. 32
30 Relative pin power distribution calculated from Polaris for the BWR transition core at BOC and EOC, wherein a twice-burned LEU assembly (NW) is surrounded by fresh ATF assemblies at 8.0 w/o ^{235}U (SE) and 10 w/o ^{235}U (SW and NE). 32
31 Differences in relative pin power for Polaris/PARCS vs. Polaris for the BWR LEU-to-ATF transition cycle 32
32 k_{eff} comparison for transition models for BWR multi-assembly model compared between Polaris and PARCS for each burnup step; cycle boundaries occur at 600 and 1200 EFPD, with the transition core reload occurring at 1200 EFPD. Shaded regions indicate (light orange) nominal core loading and (light blue) twice-burned LEU assemblies surrounded by three LEU+ assemblies. 34
33 (top) Doppler temperature coefficient (DTC) for the Polaris BWR 2 × 2 assembly model transition cycle for the LEU-to-LEU, LEU-to-LEU+, and LEU-to-ATF/LEU+) assemblies (bottom) Difference in DTC relative to the LEU-to-LEU transition core. 35

34 Quarter-core map of a BWR core with three cycles of fuel loading, modeled in PARCS. The numbering (and cell colors) represent the number of previous irradiation cycles for each fuel assembly. 36
35 BOC relative core power distribution for LEU-only, extended enrichment (LEU+), and ATF with extended enrichment core loadings. 37
36 EOC relative core power distribution for LEU-only, extended enrichment (LEU+), and ATF with extended enrichment core loadings. 38

37 DTCs and relative difference to the LEU core (ΔDTC) for the BWR full-core model over the 20-month transition cycle for the LEU-to-LEU, LEU-to-LEU+, and LEU-to-ATF cores, assuming 10 $^{w}/_{o}$ ^{235}U enrichment for LEU+ / ATF assemblies. 39
38 CBW and relative difference to the LEU core (ΔCBW) for the BWR full-core 20-month cycle model for the low-enriched uranium (LEU)-to-LEU, LEU-to-LEU+, and LEU-to-accident-tolerant fuel (ATF) cores over the 20-month transition cycle, assuming 10 $^{w}/_{o}$ ^{235}U LEU+ / ATF assemblies. 40

39 2×2 lattice with nominal pins and one enlarged pin (NW corner) used for testing power normalization against TRITON/NEWT. A–2

LIST OF TABLES

1 Energy group boundaries for PARCS 2G, 4G, and 8G structures 3
2 Specification of PWR lattice design modeled in Polaris 5
3 Specification of BWR lattice design modeled in Polaris 7
4 Uranium enrichment and gadolinia concentration for each type of fuel pin in the Polaris BWR assembly models 7

5 Verification of Polaris/PARCS for the PWR LEU and LEU+ multi-assembly model (all fresh assemblies) as compared to Polaris for the PARCS few-group models and Serpent CE model. 10
6 Characteristics of the PWR LEU to LEU transition core (depleted LEU assembly surrounded by fresh LEU assemblies) as compared to Polaris for the PARCS few-group model. 11
7 Characteristics of power peaking for Polaris vs. Polaris/PARCS calculations for the LEU-to-LEU PWR transition cycle: difference in relative power for the maximum power pin in each model, peak pin location, and the difference in relative pin power at the location of the maximum power pin from Polaris. 13
8 Characteristics of the PWR LEU to LEU+ transition core (depleted LEU assembly surrounded by fresh LEU+ assemblies) as compared to Polaris for the PARCS few-group model. 14
9 Characteristics of power peaking for Polaris vs. Polaris/PARCS calculations for the LEU-to-LEU+ PWR transition cycle: difference in relative power for the maximum power pin in each model, peak pin location, and the difference in relative pin power at the location of the maximum power pin from Polaris. 16
10 Characteristics of the PWR LEU to ATF transition core (depleted LEU assembly surrounded by fresh ATF assemblies) as compared to Polaris for the PARCS few-group model. 17
11 Characteristics of power peaking for Polaris vs. Polaris/PARCS calculations for the LEU-to-ATF PWR transition cycle: difference in relative power for the maximum power pin in each model, peak pin location, and the difference in relative pin power at the location of the maximum power pin from Polaris. 17

12 Relative power distribution and k_{eff} difference for the LEU/LEU+ BWR multi-assembly transition model (all fresh assemblies, LEU surrounded by LEU+) at BOC and nominal void condition for different energy group structures 23
13 Relative power distribution and k_{eff} difference for the BWR multi-assembly lattice (all fresh assemblies, LEU surrounded by LEU+) at BOC and high-void condition for different energy group structures 26
14 Characteristics of the BWR LEU-to-LEU transition core (depleted LEU assembly with fresh LEU assembly neighbors) relative to Polaris for the PARCS few-group model. 27
15 Characteristics of power peaking for Polaris vs. Polaris/PARCS calculations for the LEU-to-LEU BWR transition cycle: difference in relative power for the maximum power pin in each model, peak pin location, and the difference in relative pin power at the location of the maximum power pin from Polaris. 28
16 Characteristics of the BWR LEU-to-LEU+ transition core (depleted LEU assembly surrounded by fresh LEU+ assemblies) as compared to Polaris for the PARCS few-group model. 29
17 Characteristics of power peaking for Polaris vs. Polaris/PARCS calculations for the LEU-to-LEU+ BWR transition cycle: difference in relative power for the maximum power pin in each model, peak pin location, and the difference in relative pin power at the location of the maximum power pin from Polaris. 30

18 Characteristics of the BWR LEU-to-ATF transition core (depleted LEU assembly with fresh ATF assembly neighbors) relative to Polaris for the PARCS few-group model. 31
19 Characteristics of power peaking for Polaris vs. Polaris/PARCS calculations for the LEU-to-ATF BWR transition cycle: difference in relative power for the maximum power pin in each model, peak pin location, and the difference in relative pin power at the location of the maximum power pin from Polaris. 33
20 Radial assembly power peaking factors at BOC and EOC for the BWR full-core transition cycles. 38
21 Pin dimensions used for 2×2 lattice test of non-uniform pin dimensions A–2
22 Relative pin powers and pin power differences for 2x2 non-uniform pin lattice test. A–3

ACRONYMS

ADF	assembly disadvantage factor
ARMOR	Abrasion Resistant, More Oxidation Resistant
ATF	accident-tolerant fuel
BOC	beginning of cycle
BWR	boiling water reactor
CBW	control blade worth
CE	continuous energy
CRW	control rod worth
DTC	Doppler temperature coefficient
EFPD	effective full-power days
EOC	end of cycle
FG	few group
GNF	Global Nuclear Fuels
HALEU	high-assay low-enriched uranium
HBU	high burnup
HFP	hot full power
IFBA	integral fuel burnable absorber
LEU	low-enriched uranium
LWR	light water reactor
MG	multi-group
MOC	Method of Characteristics
NRC	U.S. Nuclear Regulatory Commission
pcm	percent mille
PPF	power peaking factor
PWR	pressurized water reactor
RFA	robust fuel assembly
WABA	wet annular burnable absorber

EXECUTIVE SUMMARY

Commercial light water reactor (LWR) operators and fuel vendors are currently interested in increasing the low-enriched uranium (LEU) fuel enrichments from the current limit of 5.0 w/o ^{235}U up to 10 w/o ^{235}U (referred to as "LEU+") in their current fleets; they are also interested in using accident-tolerant fuel (ATF) with both LEU and LEU+ fuel. This report aims to identify modeling challenges and accuracy concerns in transition core analysis using the SCALE Polaris lattice physics code [1], [2] and U.S. Nuclear Regulatory Commission core simulator PARCS [3].

At the time this study was started, no publicly available LEU+ core designs existed for boiling water reactor (BWR) or pressurized water reactor (PWR) systems. Therefore, fuel lattices were shuffled within a multi-assembly model to mimic neutronically challenging lattice combinations seen in transition cores, such as a fresh LEU+ lattice next to depleted LEU lattices. In addition to multi-assembly models, whole-core BWR transition core calculations were performed for ATF and LEU+ fuel using an existing Hatch-1 Cycle 3 core model [4]. A whole-core BWR model was chosen due to the more heterogeneous core designs compared to those for a PWR core. Since the original core is an old checkerboard core design and no core or fuel design optimization was performed for the modeled fuel types, these core calculations were intended only to provide:

- Comparisons of core characteristics of interest, such as the pin power distributions and peaking factors, Doppler temperature coefficients (DTCs), and control blade worths (CBWs) under challenging core designs,
- Identification of reactor physics challenges in modeling LEU+ and ATF cores,
- A stress test for the Polaris/PARCS two-step modeling approach, including characterization of the relative accuracy for predicting characteristics of interest such as pin power distributions.

As a secondary means of validating the Polaris/PARCS multi-assembly models, high-fidelity continuous energy (CE) Monte Carlo calculations were performed using Serpent [5] on equivalent lattice models. The pin-wise powers for the Polaris/PARCS and Serpent models were compared with the Polaris lattice model to establish the consistency of the pin power distribution across the different multi-assembly models. Finally, the effect of using additional coarse-energy groups (four and eight groups) was investigated with PARCS to determine what (if any) gains in accuracy could be realized when compared to Polaris.

The fuel lattices used for this study are based upon previously designed fuel lattices in Phase 1 studies [6], [7], with minor modifications to the BWR design to achieve a practical cycle length and lower overall power peaking factor (PPF). These original assemblies include a standard Westinghouse 17×17 PWR fuel with 6.5 w/o ^{235}U and 8 w/o ^{235}U enrichment LEU+ lattice designs and GE-14 10×10 BWR fuel designs with 8.0 w/o ^{235}U maximum (7.0 w/o ^{235}U average) and 10.0 w/o ^{235}U maximum (8.7 w/o ^{235}U average) enrichment maps. On the other hand, PWR fuel with uniform 5.0 w/o ^{235}U enrichment and BWR fuel with a 5.0 w/o ^{235}U maximum (4.4 w/o ^{235}U average) enrichment map were used in modeling of LEU fuel. Modifications to the BWR lattice include increasing the maximum Gd loadings up to 11 w/o (from 2.9 w/o maximum) and updating the assembly enrichment maps.

In combination with LEU+ fuel, Al_2O_2 and Cr_2O_3-doped PWR fuel and BWR fuel with FeCrAl cladding ATF fuel were tested in multi-assembly models and by way of full-core analysis (BWR only) for comparison and stress testing analysis procedures.

Based on the core characteristics of interest compared in this study, such as the power distribution, DTCs, and control rod worths (CRWs) at hot full power (HFP) conditions, the results of the PWR and BWR multi-assembly models, and BWR full-core model can be summarized as follows.

1. At beginning of cycle (BOC), the pressurized water reactor (PWR) and boiling water reactor (BWR) multi-assembly models in PARCS were verified to agree in eigenvalue and power distribution compared to Polaris and Serpent Monte Carlo results. The number of coarse energy groups used in the PWR and BWR models (e.g., 2, 4, and 8 energy groups) has a negligible effect on the discrepancy introduced between PARCS and Polaris.
2. For the transition cycle analysis in the PWR and BWR multi-assembly models, the eigenvalue results from PARCS and Polaris agree within 100 percent mille (pcm) over the full transition cycle.
3. In the PWR and BWR multi-assembly models in general, the transition to LEU+ and the use of ATF designs reduce CRW and DTC. Differences in reactivity coefficients between ATF and LEU+ are negligible and are consistent with Phase I study findings.
4. The results for BWR whole-core transition models suggest that the changes in CBW and DTC have similar trends and magnitudes to those of the multi-assembly models.
5. In the BWR whole-core model, the introduction of the LEU+, ATF, and ATF transition cycles results in an increase in the the magnitude of the PPF, and the largest increase was observed in the LEU+ transition model.

In modeling the LEU-to-ATF systems using Polaris as multi-assembly models, we additionally made two observations which are important to note.

1. First, pin powers reported by Polaris are a *volumetric* tally; i.e., pin powers normalized per unit area/volume. While in most multi-assembly cases in which the pin volumes are equal. However, for the BWR LEU-to-ATF transition core, the ATF assembly fuel radius is larger than the corresponding LEU pins, necessitating renormalization of the pin power output by the relative pin volumes to the system-average volume in order to make a direct comparison of pin powers to PARCS. Users should thus be cautioned when making power comparisons with multi-assembly models using non-uniform pin sizes. This is discussed in greater detail in Section 4.5.
2. Second, current methods implemented in Polaris intended for removing sub-assembly materials (such as burnable absorbers) may not be appropriate for representing the swapping of entire fuel assemblies within a multi-assembly model, particularly if the pin design dimensions are not identical for the replacement assembly. An example of this would be using the swap capability to represent an LEU-to-ATF transition cycle, wherein depleted LEU assemblies are replaced by fresh ATF assemblies within the multi-assembly model. In this case, because the fuel radius is larger in the ATF design than the LEU assembly, the total heavy metal mass will change, producing an inaccurate power normalization. It should be noted however that the net effect of the mass difference is comparably smaller than the error introduced by failing to account for differences in individual pin volume (discussed in the previous item).

Finally, future development and enhancement needs for Polaris and PARCS have been identified based on these findings.

ACKNOWLEDGMENTS

Support for this work was provided by the US Nuclear Regulatory Commission Offices of Nuclear Regulatory Research, Nuclear Reactor Regulation, and Nuclear Material Safety and Safeguards. The authors would also like to thank Dr. Andrew Ward of the University of Michigan for his help with PARCS usage and Dr. Yunlin Xu of Purdue University for his valuable feedback on this work.

1. INTRODUCTION

Commercial light water reactor (LWR) vendors and operators plan to include accident-tolerant fuel (ATF) designs that incorporate enrichments higher than 5.0 w/o ^{235}U (referred to as low-enriched uranium (LEU)+) in the current fleet of nuclear power plants. The term LEU+ in this context is used to refer to enrichments between 5.0 w/o ^{235}U and 10.0 w/o ^{235}U, a subset of the category of high-assay low-enriched uranium (HALEU) being considered for use in commercial LWRs and advanced reactor designs. The main goal of additional fuel enrichment in LEU+ fuel designs (5.0 – 10.0 w/o ^{235}U) is to improve fuel economy in the current reactor fleet, enabling higher burnup than that of typical reactor fuels [6], [7]. ATF designs are used to improve the safety level of the fuel system under accident conditions [8].

Several types of ATF designs are being developed by various industry vendors for either near- or longer-term deployment. These designs include chromium-coated cladding, FeCrAl cladding, and doped fuels. Westinghouse is developing Advanced Doped Pellet Technology in chromium-coated zirconium alloy cladding [9]. Framatome, on the other hand, continues to develop chromium-coated M5 cladding with chromia-enhanced uranium oxide [10]. Global Nuclear Fuels (GNF) is developing FeCrAl alloy cladding and Abrasion Resistant, More Oxidation Resistant (ARMOR) coating design for zirconium alloys [11].

Economic analysis of the ATF designs on an LWR-type reactor core suggests that the ATF implementation has a positive effect on fuel cycle economics. The favorable effects are seen not only in the equilibrium ATF core but also in the transition cycle from standard fuels. Further improvement is also observed in the economic analysis of the 24-month transition cycle, which will be the recommended path in future LWR development [12].

However, adoption of LEU+, ATF, and high burnup (HBU) fuels in the U.S. commercial fleet requires a clear understanding of the effects on core physics parameters and used fuel isotopic content, as well as confidence in the accuracy of computer code predictions over an expanded range of materials, enrichments, and burnups. As a part of ongoing work sponsored by the U.S. Nuclear Regulatory Commission (NRC) to prepare and support the deployment of ATF and LEU+ fuels in selected LWR designs, Phase I of this project focused on evaluating lattice physics parameters and fuel isotopic changes for standard boiling water reactor (BWR) [6] and pressurized water reactor (PWR) [7] models. Two reports have been published for the LEU+ designs for those two models, and another report focusing on the ATF features has been published [10]. Phase II of this project studied the impacts on core characteristics in steady state due to use of LEU+ fuels in both PWRs and BWRs.

The Phase I studies were conducted on the assembly-level assessment using SCALE [1] for LEU+ and ATF designs in PWR and BWR lattices. In summary, no anomalous trend was observed in the study because the LEU+ and ATF implementation resulted in expected effects. Some ATF designs, such as those employing FeCrAl cladding, introduced a reactivity penalty and should thus be considered in the fuel designs [10].

This report represents part of the Phase II efforts to investigate the core-level performance of ATF and LEU+ fuels in a transition cycle using the NRC's PARCS core simulator [3]. Because no LEU+ core designs (including fuel designs) were publicly available for either PWR or BWR systems when this study was first started, this study draws upon prior, parallel efforts to design and optimize LEU+ fuel assemblies [13], [14] as a reference design for fuel cycle and safety analysis studies. Using these designs, this report aims to model challenging core configurations that may be encountered during a transition cycle with respect to core power distributions, pin peaking factors, reactivity coefficient, as well as PARCS core simulator's ability to accurately calculate these parameters.

The key objectives of this investigation are thus 1) to provide a characterization of the behavior of significant reactor physics quantities of interest resulting from a transition to LEU+ / ATF core, including control rod worths (CRWs), Doppler temperature coefficients (DTCs), and the distribution of pin powers and corresponding peaking factors, 2) to identify significant reactor physics challenges in modeling the transition to ATF cores, including limitations to present analytical methods, and 3) to characterize the relative accuracy of the Polaris/PARCS two-step method for predicting quantities of interest such as pin power distributions.

For each of the transition cores, a multi-assembly model was analyzed in addition to a full-core model for the BWR transition cycle. Some core parameters such power distribution, CRW, and DTC are compared between the LEU and transition cores. The SCALE/Polaris code [2], which was used for the previous lattice physics work, is used here to provide the homogenized few-group constants for PARCS. To test and validate the Polaris/PARCS two-step method for analyzing factors such as the pin power distribution, each of the supercell models was compared to a lattice physics and depletion calculation using Polaris multi-lattice models and a high-fidelity continuous energy (CE) Monte Carlo calculation using Serpent [5]. It bears noting that Serpent is being employed as a secondary check upon the validity of the pin power distributions produced by Polaris rather than as a "ground truth," as the goal of this exercise is to evaluate the effect of different coarse-group energy boundary sets on the accuracy of the Polaris/PARCS solution. As such, the function of the Serpent comparison here is to validate the Polaris multi-group (MG) model used for few-group cross-section generation (used by PARCS).

A challenging feature of nodal core modeling for transition cores is in the pronounced neutronic differences between depleted LEU assemblies and adjacent fresh LEU+ or ATF assemblies with LEU+ enrichment levels (hereinafter simply referred to as ATF assemblies), which would be loaded adjacent to less reactive fuel assemblies. Therefore, a significant component of this analysis is characterizing the degree to which such challenges present issues for nodal modeling in transition cores—namely, by characterization of the relative errors in assembly-wise and pin-wise powers as compared to a reference lattice physics calculation.

A limitation to the analytical approach outlined above is the inability to capture spatial effects such as axial lattice variations (including features such as axial reflectors and partial length rods, partial control rod insertion, etc.) and thermal hydraulic feedbacks. However, these aspects are well beyond the scope of the goals of this study. Thus, the results presented are not intended to represent characteristics of an optimized commercial transition core but rather to provide prospective guidance for new challenges introduced by ATF transition cores and the capabilities of current methods to address these challenges.

2. ASSEMBLY MODELS

In this section, the multi-assembly models for the PWR and BWR representing transition cores are presented. Each represented lattice was modeled using SCALE/Polaris v6.3-Beta16 [2] with the SCALE ENDF/B-VII.1 56-group library [1]. From the Polaris calculations, few group (FG) homogenized cross sections (2G, 4G, and 8G) were generated to be utilized by PARCS [3], the bounds of which are presented in Table 1. PARCS v3.4.2 was used for all nodal calculations for the assembly and core models. Finally, Serpent v2.1.32 [5] was used to perform CE Monte Carlo calculations for the PWR and BWR supercell models to provide independent verification of pin power distributions and k_{eff} values produced by Polaris and Polaris/PARCS.

Table 1. Energy group boundaries for PARCS 2G, 4G, and 8G structures

Energy (eV)				
Upper	Lower	8G	4G	2G
$2.000 \cdot 10^7$	$1.850 \cdot 10^6$	g_1		
$1.850 \cdot 10^6$	$8.611 \cdot 10^5$	g_2	g_1	
$8.611 \cdot 10^5$	$1.700 \cdot 10^4$	g_3		
$1.700 \cdot 10^4$	117.5	g_4	g_2	g_1
117.5	5.000	g_5		
5.000	0.625	g_6	g_3	
0.625	0.150	g_7	g_4	g_2
0.150	$1.0 \cdot 10^{-5}$	g_8		

2.1 POLARIS PWR ASSEMBLY MODEL

A standard Westinghouse 17 × 17 PWR assembly with robust fuel assembly (RFA) dimensions and no integral fuel burnable absorber (IFBA) pins is modeled in Polaris with ¼ south-east symmetry as presented in Figure 1. For simplicity, the assembly gap surrounding the fuel lattice is neglected in all PWR lattice models[1]. Three different enrichment levels are constructed: 5.0 w/o ^{235}U, 6.5 w/o ^{235}U, and 8.0 w/o ^{235}U enrichment uranium oxide fuels. Each assembly model assumes a soluble boron concentration of 1,000 ppm (representing startup boron concentrations). Table 2 presents the detailed specifications of the PWR lattice. Note that each of the PWR models uses Zircaloy-4 cladding; while most commercial PWR assemblies have now graduated to using more advanced zirconium-based alloys (e.g., Alloy M5), these alloys are sufficiently similar neutronically as to introduce negligible differences for this analysis.

In addition to different enrichment levels, the ATF models are included in the assembly design. In the design specifications shown in Table 2, the ATF pins include a small amount of metal oxide dopant (Al_2O_2 and Cr_2O_3) within the UO_2 fuel. Advantages of this dopant include greater densification and grain size during fuel sintering, leading to lower fuel densification during irradiation [8]. The net result of these effects may include higher achievable fuel burnups and a lower probability of pellet–clad interaction and, ultimately, a lower likelihood of fuel failure [8].

[1] Hall *et al.* assumed an inter-assembly pitch of 21.5 cm in the Phase I PWR models [7] compared to a pitch of 21.42 cm assumed herein, resulting in an assembly gap difference of 0.04 cm. We believe this difference to be inconsequential to this analysis.

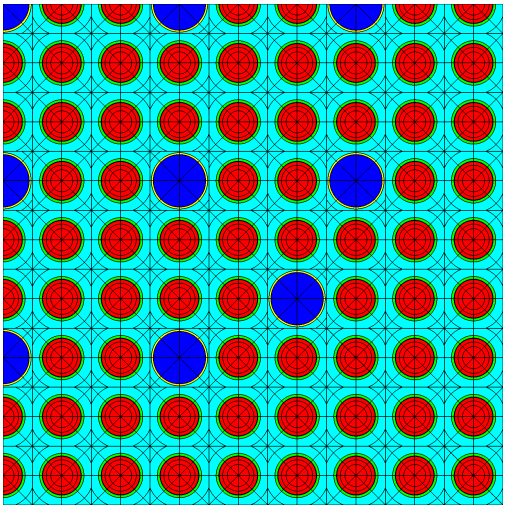

Figure 1. Westinghouse PWR 17×17 **quarter assembly, showing fuel pins (red) and coolant guide tube (blue).**

Combining with the extended enrichment models, three types of PWR lattice are modeled in Polaris: a nominal LEU assembly, LEU+, and ATF. The LEU+ and ATF also have two different enrichment levels: 6.5 $^{w}/_{o}$ ^{235}U and 8.0 $^{w}/_{o}$ ^{235}U. These variations are used in the transition modeling to determine the effect of adding advanced fuel types in the reactor physics calculation for PWR cores.

To obtain various reactor physics parameters to compare in later core physics calculations, the Polaris model includes corresponding branched calculations, which include a control rod map (inserted and withdrawn) and fuel temperatures (nominal and high temperature: 950 and 1500 K, respectively). Each of the fuel assembly models is depleted with a power of 40 megawatts per metric ton of initial heavy metal $\left(\frac{\text{MW}}{\text{MTU}}\right)$ to a discharge burnup of 80 gigawatt-days per metric ton of initial uranium $\left(\frac{\text{GWd}}{\text{MTU}}\right)$. The branched, burned, few-group–homogenized cross sections are stored in `.t16` files by Polaris, which can later be converted to PMAXS [15] cross section files formatted for PARCS.

2.2 POLARIS BWR ASSEMBLY MODEL

As explained in the previous section, this work utilized SCALE/Polaris to perform lattice calculations on assembly models and the PARCS core simulator to perform the core physics calculations. The lattice model is based on the GE-14 fuel assembly, which is a 10×10 fuel pin lattice consisting of various enrichments with two water rods.

The lattice models used are based on the dominant region of the GE-14 BWR fuel assembly design. To model the transition core in PARCS, the cross sections from different types of fuel assemblies must be generated from Polaris. Therefore, three lattice designs are modeled in Polaris: LEU, LEU+, and ATF assembly designs. Detailed parameters of the designs are presented in Table 3.

In the design specifications shown in Table 3, the ATF rods have a larger pellet radius and thinner cladding than standard LEU fuel pins; these rods are designed as such to mitigate parasitic absorption effects in FeCrAl cladding (i.e., to preserve the assembly reactivity). Thus, the larger fuel radius and thinner FeCrAl cladding layer have comparable reactivity with the LEU fuel assembly designs. The LEU+ and ATF assemblies use higher enrichment (8.0 $^{w}/_{o}$ ^{235}U or 10.0 $^{w}/_{o}$ ^{235}U max enrichment) than the non-LEU+ assembly designs.

Table 2. Specification of PWR lattice design modeled in Polaris

Parameter	LEU	LEU+	ATF
Lattice Size	17×17		
Assembly Pitch (cm)	21.42		
Fuel Rod Pitch (cm)	1.26		
Soluble boron (ppm)	1,000		
Fuel Pellet Radius (cm)	0.4096		
Gap Thickness (cm)	0.0084		
Cladding Thickness (cm)	0.057		
Cladding Material	Zircaloy-4	Zircaloy-4	Zircaloy-4 with Cr coating (3.94 at. %)
Fuel Enrichment (w/o ^{235}U)	5.0	6.5 or 8.0	6.5 or 8.0
Fuel Dopant (at. %)	–	–	Al_2O_3: 2 Cr_2O_3: 8

The lattices consist of various types of fuel rods with different ^{235}U enrichments and gadolinia concentrations shown in Table 4. In the LEU and ATF lattices, the fuel enrichment ranges from 1.6 w/o ^{235}U to 4.9 w/o ^{235}U, with some pins containing between 6.0 w/o and 8.0 w/o Gd_2O_3. For the LEU+ and ATF lattices with 8.0 w/o ^{235}U maximum enriched uranium, the fuel pin enrichment ranges from 2.6 w/o ^{235}U to 8.0 w/o ^{235}U with gadolinia concentrations of $7.0 - 11.0$ w/o. A higher level of enrichment and gadolinia concentration than the other models are used for the assembly models with 10.0 w/o ^{235}U maximum uranium enrichment. All BWR lattices are modeled with square channel boxes to maintain modeling consistency with the Polaris multi-lattice model (as explained in Section 4). The specific enrichments and gadolina weight fractions are illustrated for the LEU lattice as Figure 2 and for the 8 w/o ^{235}U and 10 w/o ^{235}U lattices (used for the LEU+ and ATF assemblies), respectively, as Figures 3 and 4.

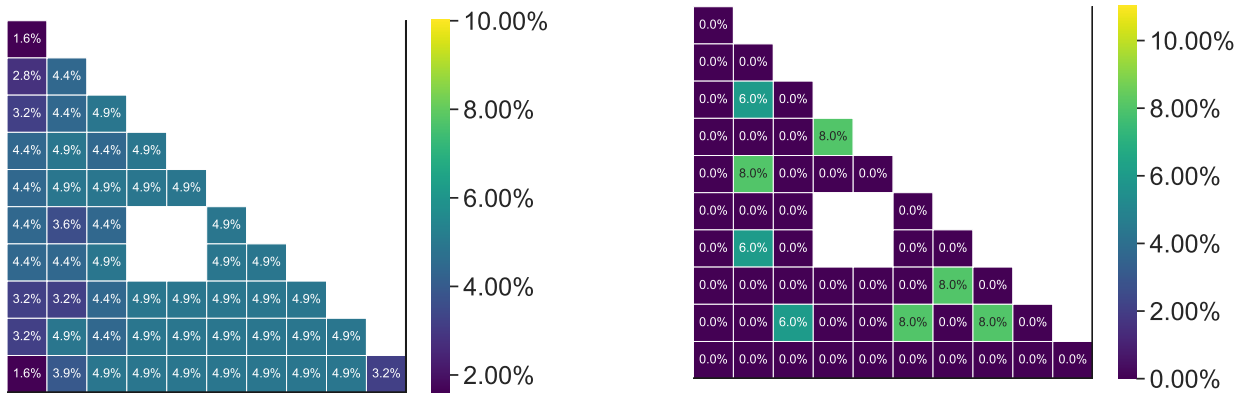

(a) Uranium enrichment **(b) Gadolinia concentrations**

Figure 2. Pin enrichments and gadolinia concentration (wt. %) for the BWR LEU assemblies used for this study

For each of the BWR lattice models, a uniform moderator void fraction of 40% was used within the channel box with a moderator temperature of 560 K and a density of 0.74 $\frac{g}{cm^3}$ for the bypass flow outside the channel box [14]. Likewise, branching calculations for control blade insertion (in/out) and fuel

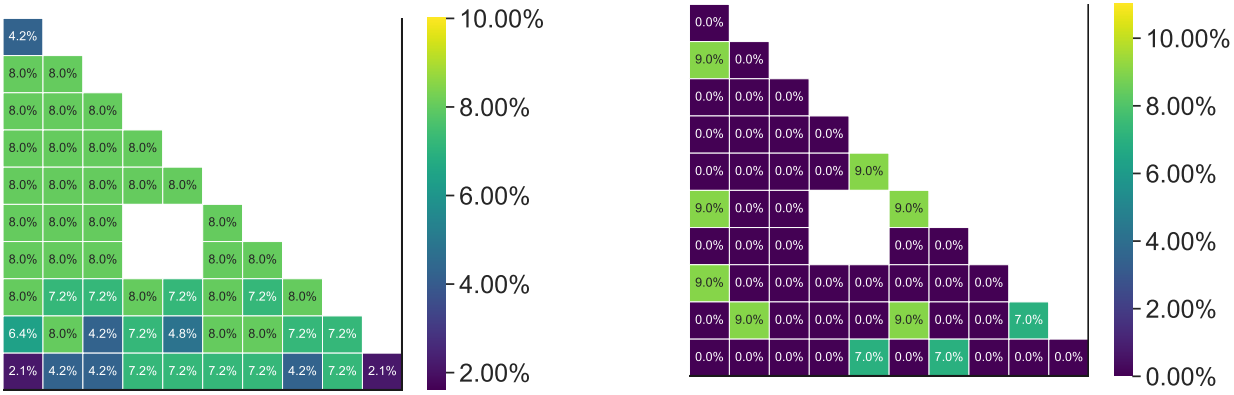

(a) Uranium enrichment **(b) Gadolinia concentrations**

Figure 3. Pin enrichments and gadolinia concentration (wt. %) for the 8 w/o ^{235}U maximum enrichment LEU+/ATF BWR assemblies used for this study

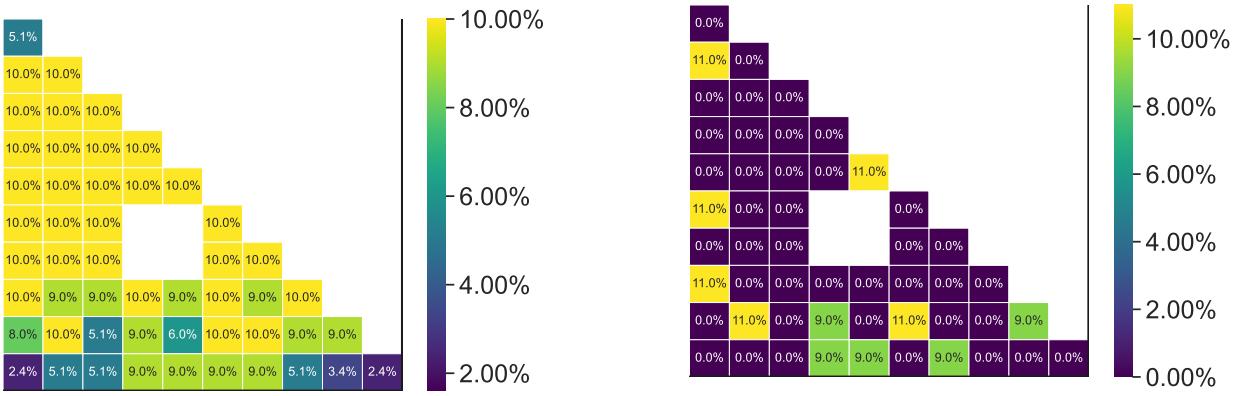

(a) Uranium enrichment **(b) Gadolinia concentrations**

Figure 4. Pin enrichments and gadolinia concentration (wt. %) for the 10 w/o ^{235}U maximum enrichment LEU+/ATF BWR assemblies used for this study

Table 3. Specification of BWR lattice design modeled in Polaris

Parameter	LEU	LEU+	ATF
Lattice Size		10×10	
Assembly Pitch (cm)		14.8945	
Wide Gap (cm)		0.9525	
Narrow Gap (cm)		0.4749	
Fuel Rod Pitch (cm)		1.2954	
Cladding Material	Zircaloy-2	Zircaloy-2	FeCrAl
Fuel Pellet Radius (cm)	0.438	0.438	0.4665
Gap Thickness (cm)	0.009	0.009	0.009
Cladding Thickness (cm)	0.066	0.066	0.0385
Fuel Enrichment ($^{w}/_{o}$ ^{235}U)			
Maximum	4.9	8.0 or 10.0	8.0 or 10.0
Average	4.4	7.0 or 8.7	7.0 or 8.7

Table 4. Uranium enrichment and gadolinia concentration for each type of fuel pin in the Polaris BWR assembly models

Maximum enrichment	$^{w}/_{o}$	Fuel 1	Fuel 2	Fuel 3	Fuel 4	Fuel 5	Fuel 6	Fuel 7	Fuel 8	Fuel 9
4.9 $^{w}/_{o}$ ^{235}U	^{235}U	1.6	2.8	3.2	3.6	3.9	4.4	4.9	4.4	3.95
	Gd	0.0	0.0	0.0	0.0	0.0	0.0	0.0	6.0	8.0
8.0 $^{w}/_{o}$ ^{235}U	^{235}U	2.15	3.25	4.25	4.8	6.4	7.2	8.0	7.2	8.0
	Gd	0.0	0.0	0.0	0.0	0.0	0.0	0.0	7.0	9.0
10.0 $^{w}/_{o}$ ^{235}U	^{235}U	2.4	3.35	5.05	6.0	8.0	9.0	10.0	9.0	10.0
	Gd	0.0	0.0	0.0	0.0	0.0	0.0	0.0	9.0	11.0

temperature (950 / 1500 K) were also performed to calculate important quantities such as DTC and control blade worth (CBW).

3. PWR MULTI-ASSEMBLY CALCULATION

3.1 PWR 3×3 MODEL

For a reference to compare with the PARCS model, a 3×3 multi-assembly model was also built in Polaris, modeled using quarter (SE) symmetry with reflective boundary conditions, as shown in Figure 5. Note that with reflective boundary conditions, the model overestimates the ratio of fresh fuel to burned fuel versus using a periodic boundary condition, which would consist of a repeating pattern of the twice-burned assembly and three adjacent (fresh) neighboring assemblies. The net result of the reflective boundary model used here is bounding/limiting compared to periodic for quantities such as DTCs and CRWs given the over-representation of fresh LEU+ and ATF relative to depleted assemblies.

To simplify the multi-assembly model, the assembly gap was removed and no IFBA layer was modeled on the pins. The Polaris and equivalent PARCS model for this case is presented in Figure 5. The models include three different PWR fuel assembly models (previously discussed in Section 2.1). To verify the PWR 3×3 multi-assembly model, three different lattices designs, with five different fuel pin designs are considered are used: the nominal 4.9 w/o ^{235}U assembly, 6.5 w/o ^{235}U assemblies, and 8.0 w/o ^{235}U assemblies, ATF with 6.5 w/o ^{235}U enrichment assemblies, and ATF with 8.0 w/o ^{235}U enrichment assemblies

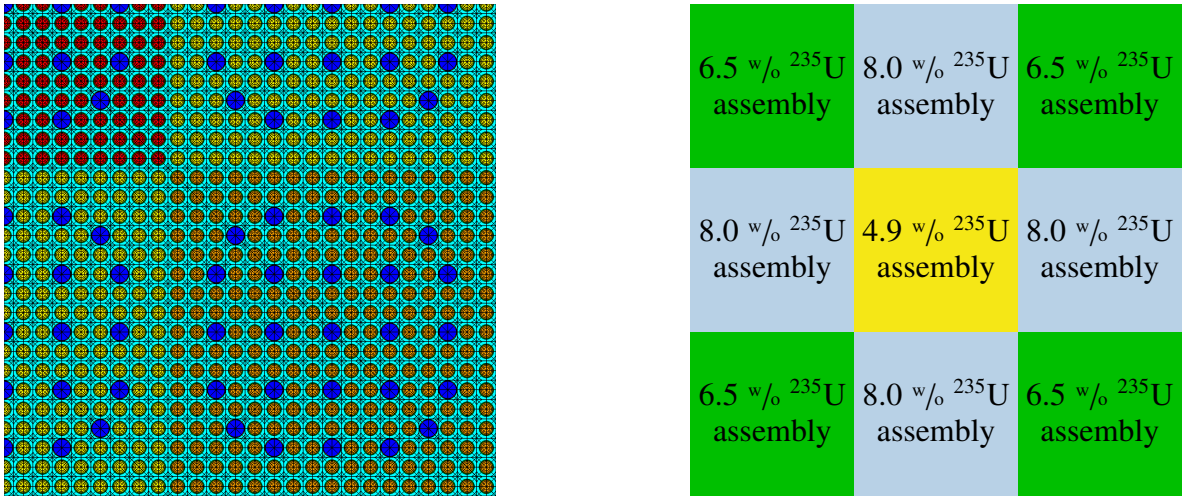

(a) Polaris 3×3 assembly model with SE symmetry

(b) 3×3 assembly model in PARCS with the assembly XS generated from Polaris

Figure 5. Multi-assembly PWR multi-assembly models used for group sensitivity study. Note that the Polaris model (left) employs quarter-core symmetry (reflective boundary conditions).

The PWR multi-assembly model was run in three 20-month reactor cycles. For each cycle, the model configuration is described as follows.

1. Initially, the model consisted of all LEU fuel assemblies containing fresh fuels with 4.9 w/o ^{235}U enrichment and Zircaloy-4 cladding. This cohort of assemblies is then burned twice (two 20-month cycles).
2. For the third cycle, the (now twice-burned) NW nominal LEU assembly are retained, and the three adjacent assemblies were replaced by fresh LEU+ assemblies to form the configuration as shown in Figure 5.

Fuel "shuffling" in Polaris is effectively achieved by specifying a new lattice map for the transition cycle (replacing the assemblies adjacent to the LEU assembly with new compositions).

For each of the three transition cycles considered (LEU-to-LEU, LEU-to-LEU+, and LEU-to-ATF), the calculation is conducted for three 20-month operational cycles. For the first and second cycles, LEU assemblies are used in Figure 5; then, on cycle three, all fuel assemblies except the middle are replaced with the fresh fuel assemblies. This configuration is selected to generate a challenging steep flux gradient for PARCS simulation between the central depleted LEU fuel and surrounding high-reactivity LEU+ and ATF) fuel assemblies. In practice, such configurations are expected to be avoided during a transition cycle, as twice burned fuel bundles are expected to be located at the periphery and not surrounded by fresh LEU+ fuel assemblies. But these models are still useful to assess the impacts of LEU+ and ATF on transition core characteristics.

Limitations of this approach include the fact that the initial multi-assembly model used for establishing the compositions of the nominal assembly after two cycles effectively relies upon a uniform core loading pattern with no IFBA or other burnable absorbers. This is a conservative assumption wherein the reactivity loading is substantially higher than that of a more realistic core, wherein the most reactive assemblies would be surrounded by once- and twice-burned assemblies; moreover, the inclusion of IFBA rods in the fresh assemblies would present a more realistic approximation.

However, modeling burnable poisons for the multi-assembly models for the transition core scenario presents numerous challenges. Although Polaris is capable of modeling features such as IFBA, the inclusion of these pins would require a much finer ray spacing for the Polaris Method of Characteristics (MOC) calculation—something that would increase computation time significantly for a three cycle simulations of a super cell geometry. Moreover, burnable poisons such as wet annular burnable absorbers (WABAs) and pyrex are not typically deployed in each assembly and moreover not in the same amount in the core (i.e., IFBAs); as such, their presence in a multi-assembly model with reflective boundary conditions would over-estimate the amount of burnable poisons introduced into the core.

The inclusion of burnable absorbers would be expected to reduce power peaking within the LEU assemblies and enable an extended cycle length (due to a lower reactivity swing); however, because the purpose of the first two cycles in this model is exclusively to establish an estimated depleted inventory for the (twice-burned) LEU assembly, the impact of not including burnable absorbers is expected to be small. Specifically, residual effects from the use of burnable absorbers within the first two (LEU-only) cycles (i.e., larger observed power peaking factors (PPFs) due to the absence of burnable absorber rods) would largely be expected to vanish over two cycles. Thus, their exclusion is expected to have a minimal effect on the calculated composition of the twice-burned LEU assemblies used for transition core analysis. With respect to the transition cycle, the absence of burnable absorbers is inherently a conservative assumption, overestimating assembly-wise PPFs and the reactivity swing over the cycle.

3.2 GROUP STRUCTURE COMPARISON FOR ALL-FRESH MULTI-ASSEMBLY MODELS

To assess the impact of the choice of energy group structures on the accuracy of the two-step Polaris/PARCS simulation, the model presented in Figure 5 is compared for different group structures used in PARCS with Polaris-generated cross sections: two-group (2G), four-group (4G), and eight-group (8G), the respective bounds of which are enumerated in Table 1. The results for this comparison are presented in Table 5, wherein the Polaris 3×3 multi-assembly result is used as the reference case for this problem. A high-fidelity, CE Monte Carlo solution using Serpent [5] was also calculated for the same geometry (using 500 histories with 500,000 particles per history and transport cross-sections from ENDF/B-VII.1) to provide a reference solution for the Polaris results; the calculated power distribution from Serpent is illustrated as Figure 7.

The multi-assembly model used for this study consists of all fresh fuel assemblies (LEU, LEU+), and ATF since the goal of this exercise is simply to evaluate the consistency of pin power estimates using Polaris/PARCS for different energy group structures for a more challenging assembly layout.

Table 5. Verification of Polaris/PARCS for the PWR LEU and LEU+ multi-assembly model (all fresh assemblies) as compared to Polaris for the PARCS few-group models and Serpent CE model.

Model	k_{eff}	Δk_{eff} (pcm)	Power difference (%) Assembly Average	Assembly Max	Pins Average	Pins Max
Polaris 3 x 3 (56G)	1.37718	–	–	–	–	–
Serpent 3 x 3 (CE)	1.37901	183	0.06	0.24	0.24	0.88
PARCS (2G)	1.37719	1	0.11	0.28	0.38	2.29
PARCS (4G)	1.37713	-5	0.23	0.39	0.64	3.16
PARCS (8G)	1.37716	-2	0.14	0.26	0.33	1.97

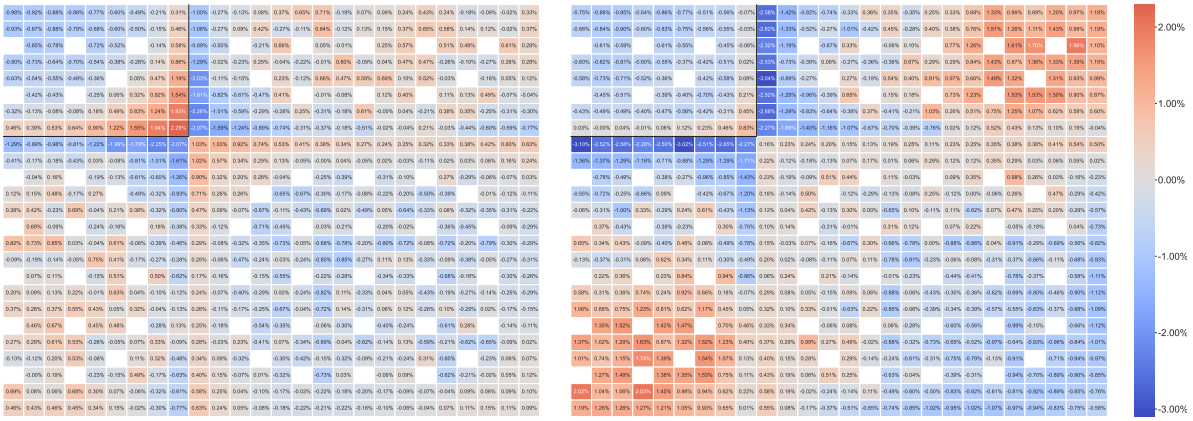

(a) 2-group PARCS **(b) 4-group PARCS**

(c) 8-group PARCS **(d) Serpent (CE)**

Figure 6. PWR 3×3 assembly model (SE symmetry) relative pin power differences for the PWR all-fresh LEU + LEU+ assembly configuration as compared to Polaris for the PARCS few-group models and Serpent CE model.

Figure 6 shows the relative differences in pin power compared to Polaris for the fresh multi-assembly

configuration (i.e., fresh LEU assembly surrounded by fresh LEU+ assemblies). Notable features include an overall decrease in the pin power error compared to Polaris for an increasing number of energy groups in PARCS, particularly around the assembly interface regions. Similarly, per Table 5, the k_{eff} error likewise decreases with an increasing number of energy groups. Overall, a very good agreement is observed for both k_{eff} and the pin power distributions for both Polaris/PARCS and the Serpent CE model (Figure 7), with a maximum error in the pin power between around 2–3% and an average error well under 1%.

Likewise, the pin power error at the assembly interfaces decreases with increasing energy groups in PARCS. Polaris and Serpent show excellent agreement for the pin power distribution; Polaris appears to slightly underestimate the powers of pins in the 8.0 w/o ^{235}U enriched assemblies (NE and SW).

3.3 LEU TO LEU CORE

As a means of qualifying the consistency between Polaris and Polaris/PARCS calculations, an additional transition LEU-to-LEU core was analyzed. This case effectively reproduces the transition core analysis performed with the LEU+ and ATF assemblies but replaces the surrounding LEU assemblies with fresh LEU assemblies instead. This cross check serves as a baseline for the Polaris to Polaris/PARCS comparisons by establishing trends observed for both power distribution as well as k_{eff} for a transition cycle with no other change in the fuel design. In other words, effects due to the change of assemblies to LEU+, and possibly also to ATF designs, can be decoupled from the bias introduced by the fuel shuffling alone.

Table 6 enumerates the relative differences in k_{eff} as well as assembly and pin power peaking factors between the Polaris and Polaris/PARCS 3×3 assembly models for the LEU to LEU transition cycle at beginning of cycle (BOC) and end of cycle (EOC).

Table 6. Characteristics of the PWR LEU to LEU transition core (depleted LEU assembly surrounded by fresh LEU assemblies) as compared to Polaris for the PARCS few-group model.

	Model	k_{eff}	Δk_{eff} (pcm)	Pin PPF	Difference in relative power (%) Assembly Average	Assembly Max	Pins Average	Pins Max
BOC	Polaris 3×3 (56G)	1.28040	–	1.210	–	–	–	–
	PARCS (2G)	1.28148	108	1.207	0.26	0.30	0.32	0.83
EOC	Polaris 3×3 (56G)	1.05841	–	1.124	–	–	–	–
	PARCS (2G)	1.05874	33	1.130	0.19	0.54	0.68	3.01

From Table 6, the Polaris and Polaris/PARCS calculations show excellent agreement for both k_{eff} at both BOC and EOC.

The pin power distributions for Polaris and Polaris/PARCS are illustrated as Figure 8, whereas the relative pin-wise power factor errors are shown as Figure 9. As expected, the relative assembly power is comparably lower in the twice-burned LEU assembly (NW). In the progression from BOC to EOC, the power distribution across the supercell moderately flattens, and the peak power diminishes in the fresh LEU assemblies.

With respect to the relative agreement of pin powers, the pin powers show better agreement at the BOC as compared to EOC. Although the Polaris/PARCS model moderately underestimates power in the twice-burned assembly at the BOC, the relative errors shift to the assembly interface regions at the EOC, with Polaris/PARCS under-predicting pin powers in the interface region around the twice-burned LEU assembly and over-predicting powers at the corners of the fresh assemblies at the EOC. As such, though

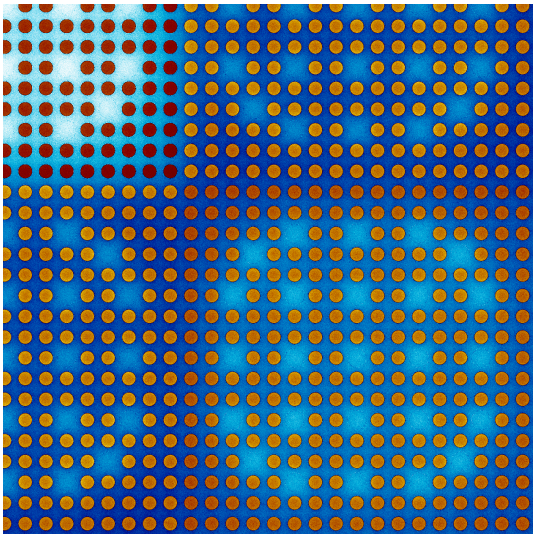

Figure 7. Serpent 3×3 PWR lattice relative fission power (red/orange) and thermal flux (blue) distribution with SE symmetry.

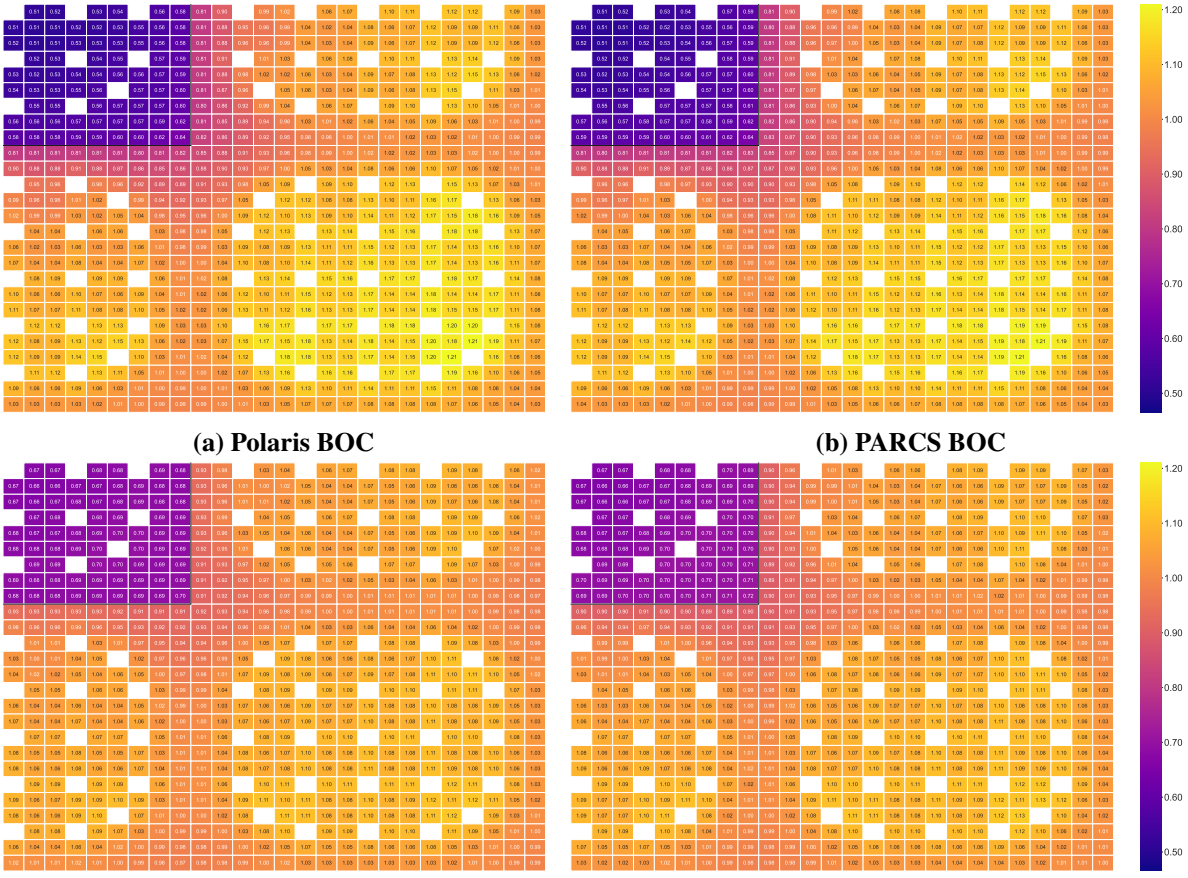

(a) Polaris BOC **(b) PARCS BOC**

(c) Polaris EOC **(d) PARCS EOC**

Figure 8. Relative pin power distribution for Polaris and Polaris/PARCS vs. Polaris for the LEU-to-LEU transition cycle

Table 6 would appear to convey superior agreement for the relative assembly powers at EOC, in fact, this result appears to be an artifact of error cancellation from the power distribution within the more reactive assemblies.

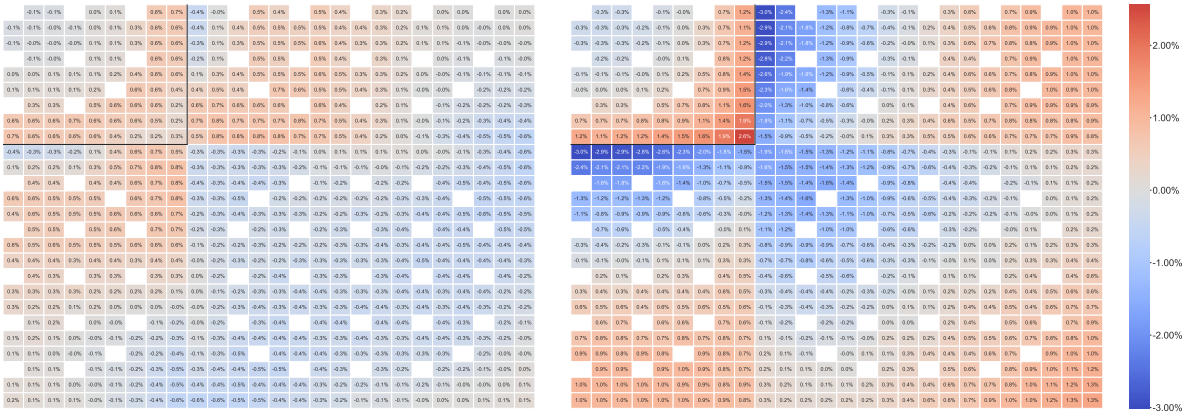

(a) BOC **(b) EOC**

Figure 9. Relative pin power differences for Polaris/PARCS vs. Polaris for the PWR LEU-to-LEU transition cycle

However, though the relative pin power difference grows relatively large in the outer regions of the fresh assemblies, the Polaris/PARCS calculation still appears to yield good agreement around the areas of the maximum pin power (i.e., the interior region of the fresh assemblies). This is evident in terms of the relatively good agreement for the calculated PPFs at both BOC and EOC. Thus, even though the relatively higher errors in pin powers are of moderate concern, the magnitude of these errors occur in regions of relatively lower power, thus decreasing the importance of the observed deviations in relative pin powers between Polaris and Polaris/PARCS.

In similar fashion, the calculated k_{eff} and relative difference between Polaris and PARCS is plotted as Figure 10. In general, PARCS shows excellent agreement with Polaris for both the initial LEU-only cycles as well as the reload cycle (cycle 3), with differences confined to 100 percent mille (pcm) or less.

An analysis of the difference in the maximum PPFs for Polaris vs. Polaris/PARCS as well as the PPF at the maximum power pin in Polaris to the corresponding location in Polaris/PARCS is presented in Table 7. Notably, Polaris and Polaris/PARCS again show excellent agreement in terms of the differences in total predicted PPF, the location of the peak power pin, and the relative power difference at the peak pin location.

Table 7. Characteristics of power peaking for Polaris vs. Polaris/PARCS calculations for the LEU-to-LEU PWR transition cycle: difference in relative power for the maximum power pin in each model, peak pin location, and the difference in relative pin power at the location of the maximum power pin from Polaris.

	ΔPPF_{max} (%)	Location of peak pin Polaris	PARCS	ΔPPF at max Polaris pin (%)
BOC	-0.31	(22,23)	(23,22)	-0.33
EOC	0.69	(22,23)	(22,23)	0.69

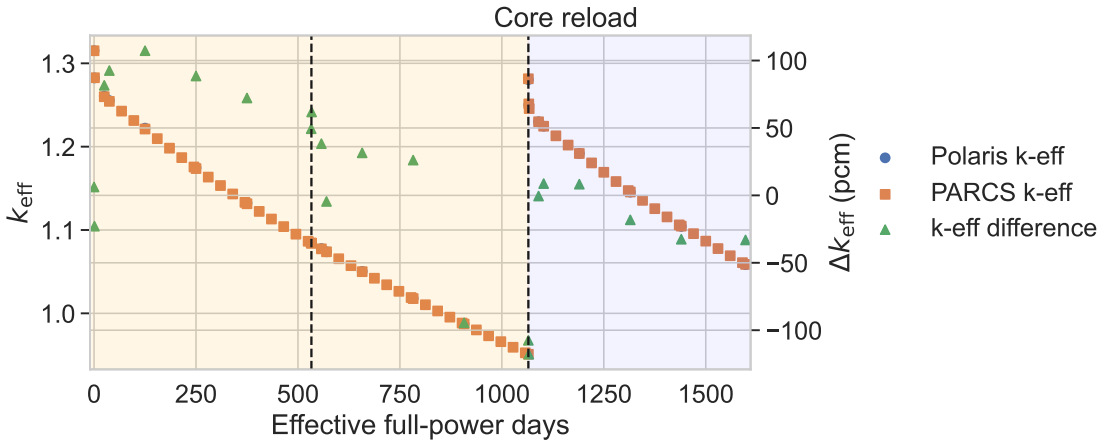

Figure 10. k_{eff} comparison for transition models for PWR 3×3 assembly model (LEU-to-LEU core) compared between Polaris and PARCS for each burnup step; cycles boundaries occur at 533 and 1065 EFPD, with the transition core reload at 1066 EFPD. Shaded regions indicate (light orange) nominal core loading and (light blue) twice-burned LEU assemblies surrounded by fresh LEU assemblies.

3.4 LEU TO LEU+ TRANSITION CORE

The second benchmark comparison consists of an LEU+ transition core wherein an LEU assembly is burned for two cycles with identical neighbors, which are then replaced with LEU+ assemblies (matching the repeated array pattern in Figure 5) with Zircaloy cladding.

Table 8. Characteristics of the PWR LEU to LEU+ transition core (depleted LEU assembly surrounded by fresh LEU+ assemblies) as compared to Polaris for the PARCS few-group model.

	Model	k_{eff}	Δk_{eff} (pcm)	Pin PPF	Difference in relative power (%) Assembly Average	Assembly Max	Pins Average	Pins Max
BOC	Polaris 3 x 3 (56G)	1.34476	–	1.204	–	–	–	–
	PARCS (2G)	1.34592	116	1.206	0.28	0.68	0.49	1.61
EOC	Polaris 3 x 3 (56G)		–	1.178	–	–	–	–
	PARCS (2G)	1.14317	39	1.187	0.15	0.80	0.60	2.19

The k_{eff} , maximum PPF, and relative assembly and pin power errors for the LEU-to-LEU+ cycle are given as Table 8. Similar to the LEU-to-LEU transition cycles, very good agreement is observed for both k_{eff} and the relative pin PPF. Likewise, a similar pattern with respect to the power distribution (Figure 11) and the distribution of pin power errors (Figure 12) as compared to the LEU-to-LEU transition cycle. In particular, the relative distribution of pin power errors show a nearly identical shape as compared to the LEU-to-LEU transition cycle with an overall very similar magnitudes of error, indicating that the pin power error distribution appears to be more of a feature of the Polaris/PARCS two-step calculation procedure rather than the specific assembly compositions.

Table 9 again provides the breakdown of the relative pin peaking factor distribution for Polaris vs. Polaris/PARCS. Much like the LEU-to-LEU transition cycle, an excellent agreement between Polaris and Polaris/PARCS is observed for the maximum difference in PPF, the location of the peak pin, and the difference in the PPF at the Polaris peak pin location.

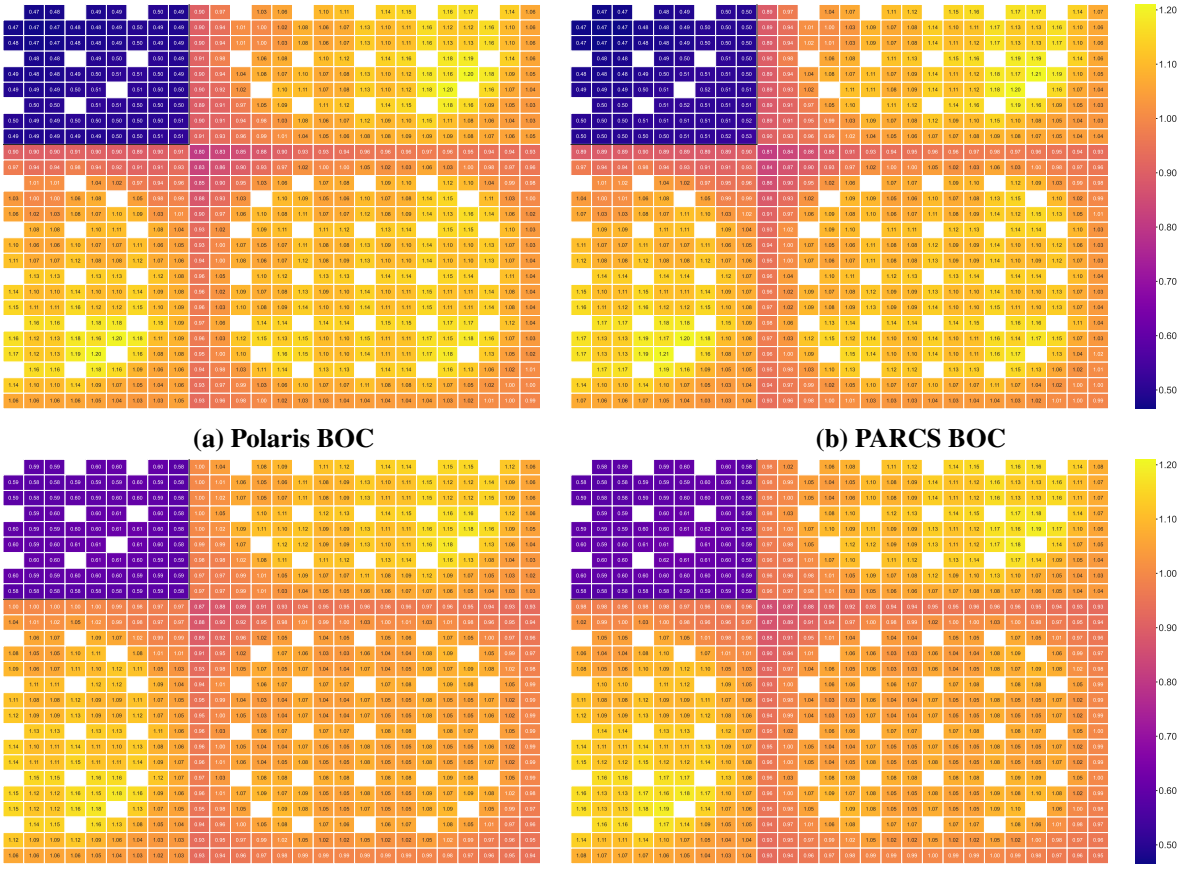

(a) Polaris BOC (b) PARCS BOC

(c) Polaris EOC (d) PARCS EOC

Figure 11. Relative pin power distribution for Polaris and Polaris/PARCS vs. Polaris for the PWR LEU-to-LEU+ transition cycle

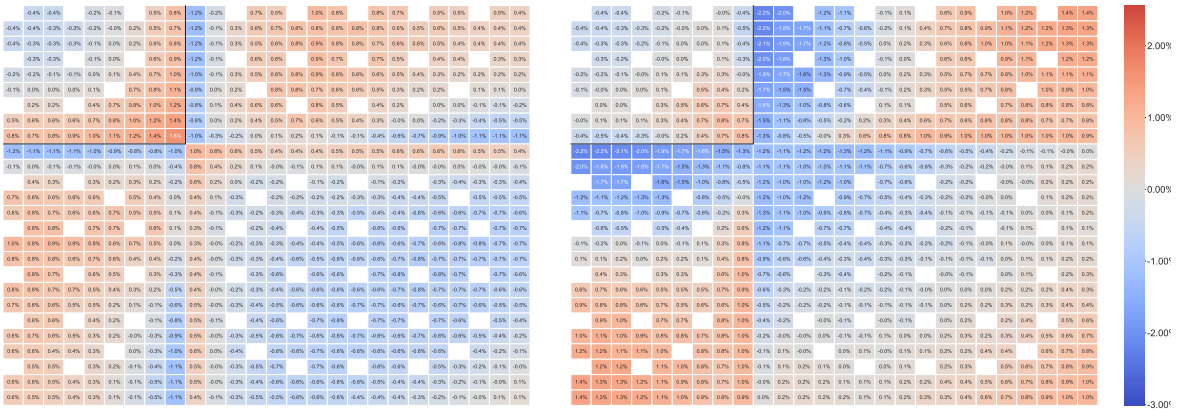

(a) BOC (b) EOC

Figure 12. Relative pin power differences for Polaris/PARCS vs. Polaris for the PWR LEU-to-LEU+ transition cycle.

Table 9. Characteristics of power peaking for Polaris vs. Polaris/PARCS calculations for the LEU-to-LEU+ PWR transition cycle: difference in relative power for the maximum power pin in each model, peak pin location, and the difference in relative pin power at the location of the maximum power pin from Polaris.

	ΔPPF_{max} (%)	Location of peak pin Polaris	PARCS	ΔPPF at max Polaris pin (%)
BOC	0.25	(5,23)	(23,5)	0.24
EOC	0.97	(5,23)	(5,23)	0.97

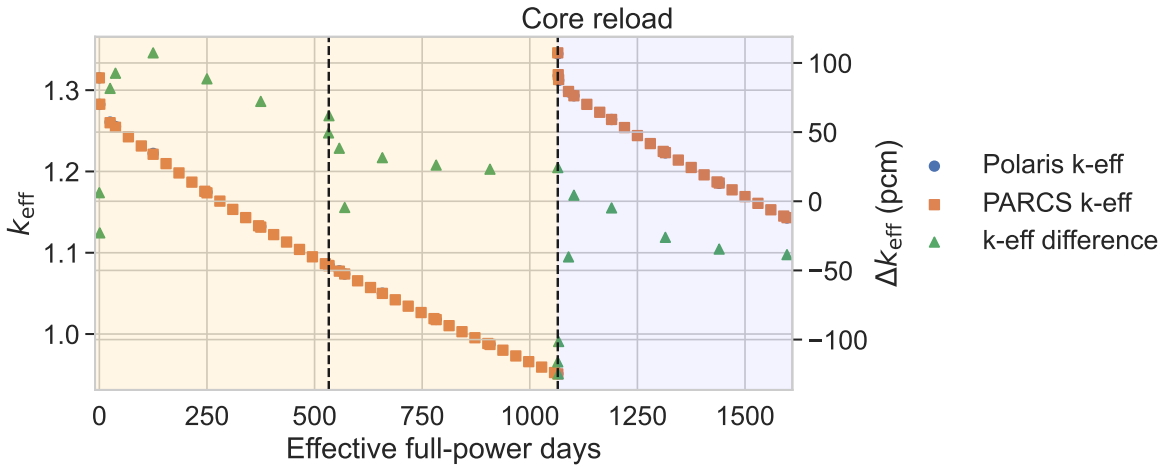

Figure 13. k_{eff} comparison for transition models for the PWR 3×3 assembly model (LEU-to-LEU+ core) compared between Polaris and PARCS for each burnup step; cycles boundaries occur at 533 and 1065 EFPD, with the transition core reload at 1066 EFPD. Shaded regions indicate (light orange) nominal core loading and (light blue) twice-burned LEU assemblies surrounded by LEU+ assemblies.

3.5 LEU TO ATF TRANSITION CORE

For the transition cycle analysis to the ATF core, the PWR multi-assembly models shown in Figure 5 are used in the calculation.

Table 10. Characteristics of the PWR LEU to ATF transition core (depleted LEU assembly surrounded by fresh ATF assemblies) as compared to Polaris for the PARCS few-group model.

					Difference in relative power (%)			
					Assembly		Pins	
	Model	k_{eff}	Δk_{eff} (pcm)	Pin PPF	Average	Max	Average	Max
BOC	Polaris 3 x 3 (56G)	1.33850	–	1.205	–	–	–	–
	PARCS (2G)	1.33966	116	1.208	0.52	1.24	0.50	1.63
EOC	Polaris 3 x 3 (56G)	1.13814	–	1.179	–	–	–	–
	PARCS (2G)	1.13852	37	1.189	0.15	0.28	0.60	2.21

Figure 16 presents the comparison of the k-eigenvalue for the PWR multi-assembly transition models with the extended-enrichment fuels transition in Cycle 3. It can be observed that the k_{eff} evolution decreases steadily in the first two cycles of operation; this is to be expected, as the assemblies are composed exclusively of fuel pins with no burnable absorbers and constant boron concentrations. After the fresh higher enrichment fuels are introduced into the model (beginning of the third cycle, around 1050 days), the k_{eff} increases dramatically, subsequently decreasing with burnup. The time-dependent k_{eff} for Polaris and Polaris/PARCS models shows excellent agreement throughout all cycles (within 100 pcm).

Table 11 provides a detailed summary of the power peaking characteristics for the ATF transition cycle. Similar to the prior PWR transition cores, once again an excellent agreement is observed for both the distribution and overall magnitude of the PPF at both BOC and EOC.

Table 11. Characteristics of power peaking for Polaris vs. Polaris/PARCS calculations for the LEU-to-ATF PWR transition cycle: difference in relative power for the maximum power pin in each model, peak pin location, and the difference in relative pin power at the location of the maximum power pin from Polaris.

	ΔPPF_{max} (%)	Location of peak pin Polaris	PARCS	ΔPPF at max Polaris pin (%)
BOC	0.27	(23,5)	(5,23)	0.26
EOC	1.00	(5,23)	(5,23)	1.00

3.6 REACTIVITY COEFFICIENTS FOR THE TRANSITION CORES

The next step of the transition cycle analysis is to compare the reactivity coefficients for different transition multi-assembly models. Three different transition cycle models are included in this procedure.

1. LEU-only: no transition is used, the LEU fuels are burned in the multi-assembly model for the first two cycles; then, on cycle three, three of the adjacent burned LEU fuel assemblies are replaced with fresh LEU fuel assemblies.
2. LEU+ transition: fresh LEU+ fuel assemblies (6.5 w/o ^{235}U and 8.0 w/o ^{235}U) replace three of the adjacent burned LEU fuel assemblies in cycle three.

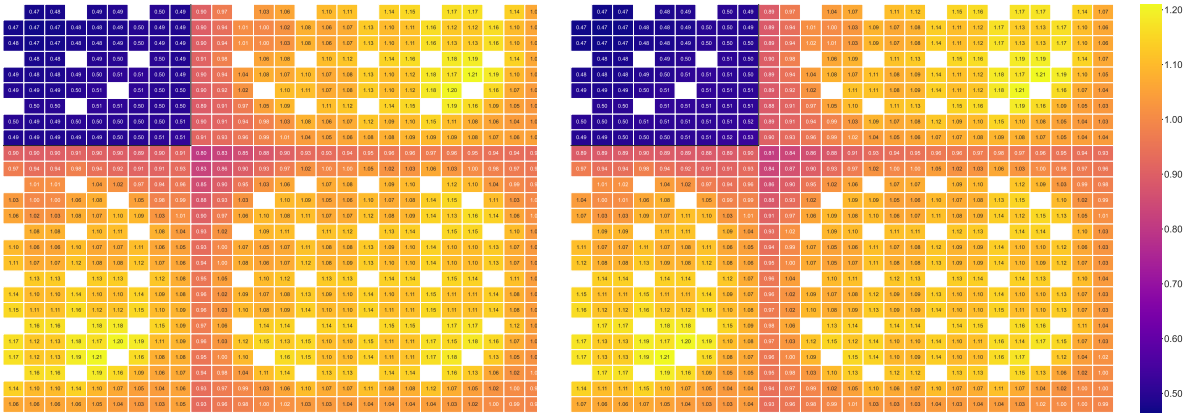

(a) Polaris BOC (b) PARCS BOC

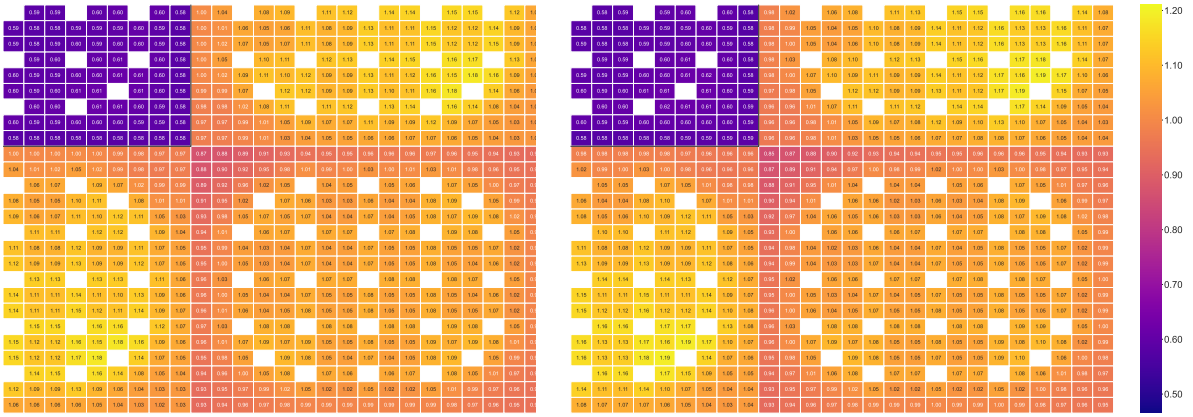

(c) Polaris EOC (d) PARCS EOC

Figure 14. Relative pin power distribution for Polaris and Polaris/PARCS vs. Polaris for the PWR LEU-to-ATF transition cycle.

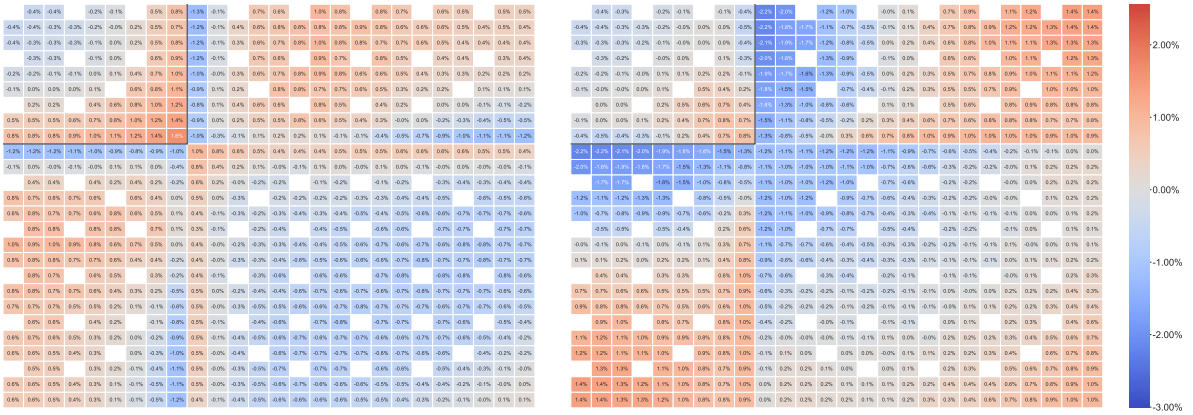

(a) BOC (b) EOC

Figure 15. Relative pin power differences for Polaris/PARCS vs. Polaris for the PWR LEU-to-ATF transition cycle.

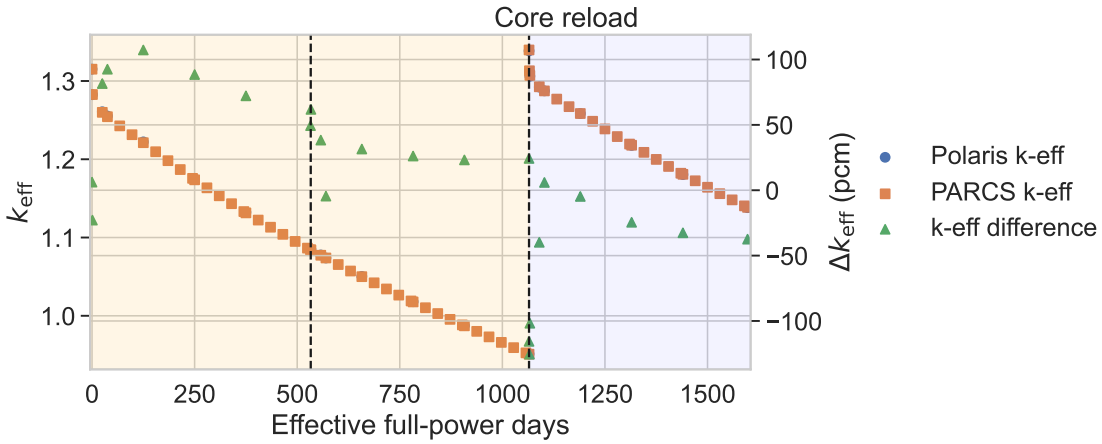

Figure 16. k_{eff} comparison for transition models for the PWR 3×3 assembly model (LEU-to-ATF core) compared between Polaris and PARCS for each burnup step; cycles boundaries occur at 533 and 1065 EFPD, with the transition core reload at 1066 EFPD. Shaded regions indicate (light orange) nominal core loading and (light blue) twice-burned LEU assemblies surrounded by ATF assemblies.

3. ATF transition: fresh ATF assemblies containing LEU+ fuel (6.5 w/o ^{235}U and 8.0 w/o ^{235}U) replace three of the adjacent burned LEU fuel assemblies in cycle three.

For each case above, the transition core modeling procedure is the same: a uniform batch of LEU assemblies is burned for the first two cycles, whereupon the three surrounding assemblies in the quarter-symmetry model are replaced in the third cycle (effectively replacing all neighboring assemblies around the twice-burned assembly).

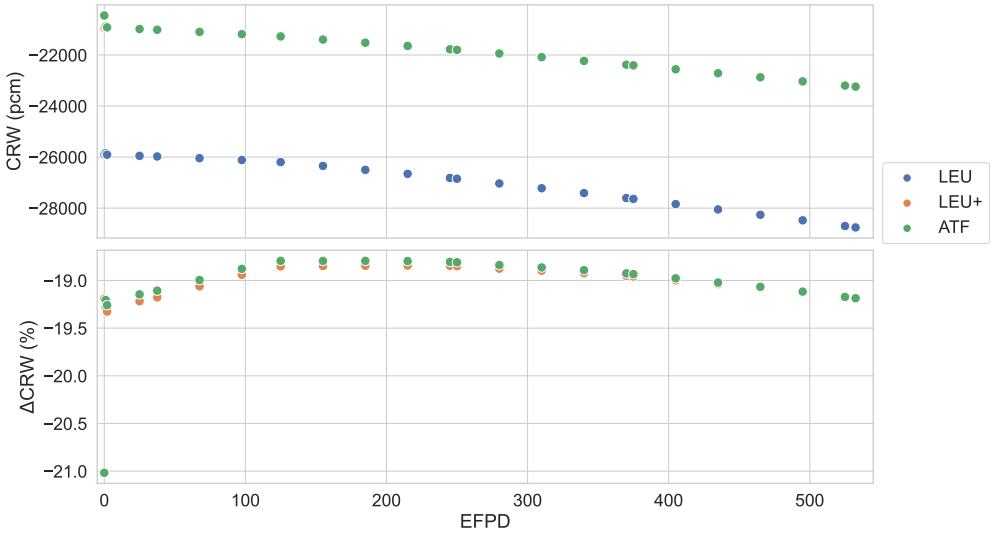

Figure 17. CRW at HFP for the 3×3 PWR assembly model in the third (transition) cycle. (Note that the LEU+ and ATF series values largely overlap.)

Based on these transition models, the CRW and the DTC at hot full power (HFP) are compared at effective full-power days (EFPD) of reactor operation in a transition cycle (cycle 3 in this model). Plots for the CRW and DTC at HFP along with burnup days for all transition models are presented in Figures 17 and 18.

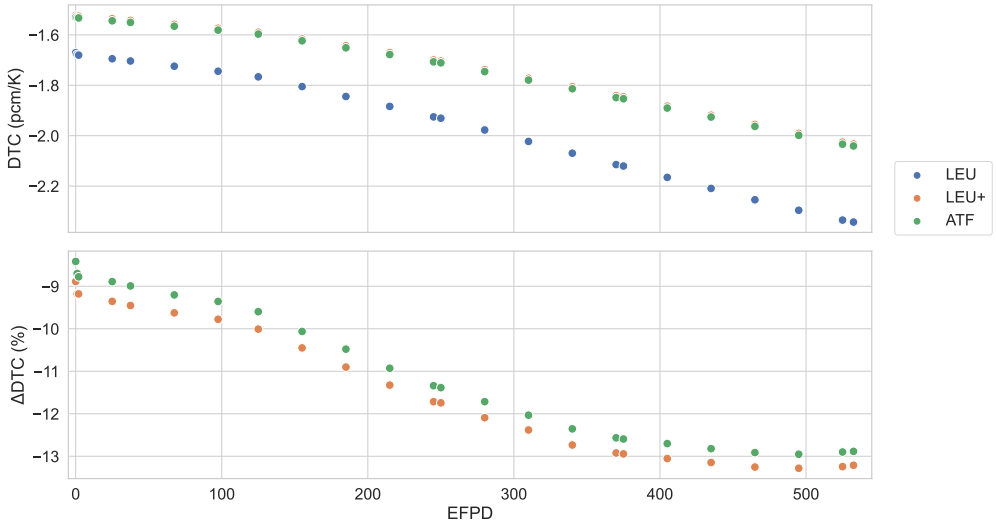

Figure 18. DTC at HFP for the 3×3 PWR assembly model in the third (transition) cycle.

Both figures show similar trends in reactivity coefficients observed in Phase 1 studies with respect to burnup. However, the reduction in reactivity coefficients with increasing enrichment is smaller than what was reported in the Phase 1 studies. The effect of dopants used in ATF is negligible, as the results for both fuel types coincide.

4. BWR MULTI-ASSEMBLY CALCULATION

4.1 BWR 2×2 MULTI-ASSEMBLY MODEL

Similar to the PWR multi-assembly models, the BWR configurations consist of a combination of LEU and LEU+ or ATF that were modeled to assess the accuracy of Polaris/PARCS two-step core simulations for anticipated fuel combinations in transition cores (Figure 19). Since BWR assemblies are required to be encapsulated inside fuel channels by design, the BWR assemblies were modeled as a 2×2 grid (again using reflected boundary conditions), taking advantage of Polaris's SVEA fuel geometry capability.

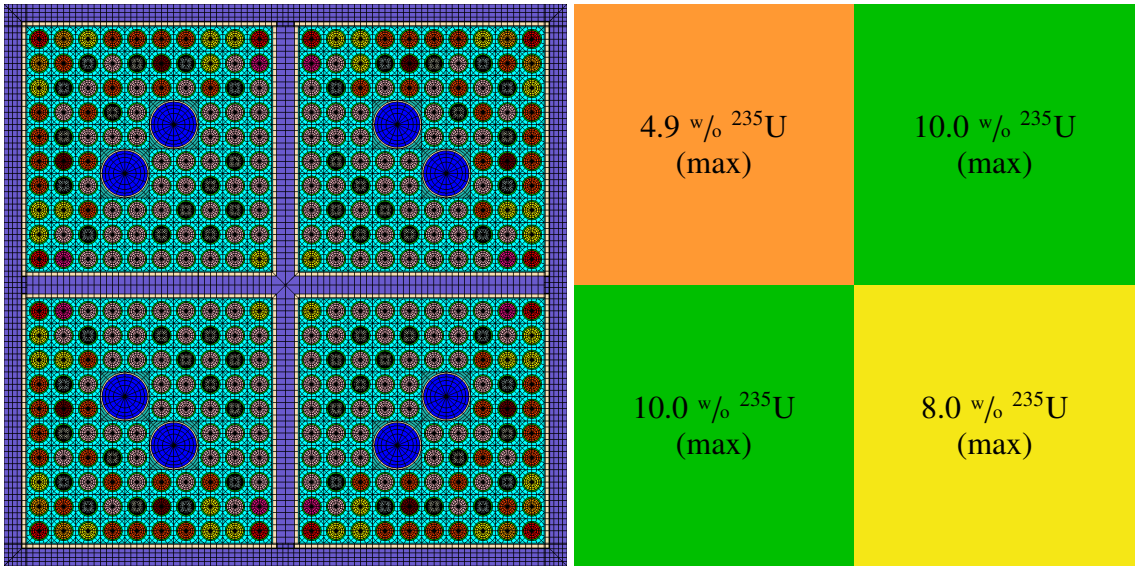

(a) Polaris 2×2 multi-assembly model

(b) PARCS 2×2 assembly model in PARCS with the assembly XS generated from Polaris

Figure 19. Multi-assembly BWR models used for group sensitivity study.

The all-fresh LEU fuel multi-assembly model was depleted for two 20-month cycles at a constant power of 25 $\frac{\text{MW}}{\text{MTU}}$ to provide depleted LEU lattices for the transition cycle. For the third (transition) cycle, the twice-burned NW LEU assembly is retained, and fresh ATF assemblies replace the three surrounding assemblies, thus producing the reflected lattice shown in Figure 19.

Likewise, the analysis for the BWR transition scenario is conducted in three stages, illustrating a nominal LEU-to-LEU transition, an LEU-to-LEU+ transition, and finally an LEU-to-ATF core, thus allowing for a separation of the effects of the transition to the ATF design from increases in the fuel assembly average enrichment.

4.2 GROUP STRUCTURE COMPARISON

Similar to the PWR fresh multi-assembly lattice, it is again useful to first consider the effects of the FG structure (enumerated previously in Table 1) on the overall accuracy of Polaris vs. Polaris/PARCS calculations for k_{eff} and the relative assembly and pin power distributions. Thus, a multi-assembly model corresponding to the assembly *enrichments* in Figure 19 was constructed using all fresh assemblies (i.e., LEU and LEU+; ATF was not considered for this exercise because it does not change the flux spectrum significantly). The resulting power distributions and k_{eff} values were then compared to Polaris for a 2G,

4G, and 8G PARCS calculation, as well as to a CE Monte Carlo model using Serpent. This was performed for two models: a nominal case (40% void) and a high-void condition (70% void within the assembly).

For comparison, the pin power distribution for the 2×2 assembly model (all fresh LEU and LEU+ assemblies) is illustrated for each condition as Figure 20. Overall, the change in relative pin powers across the lattice model is minimal between the two conditions (within a few percent) with no major regional shifts in the power distributions observed.

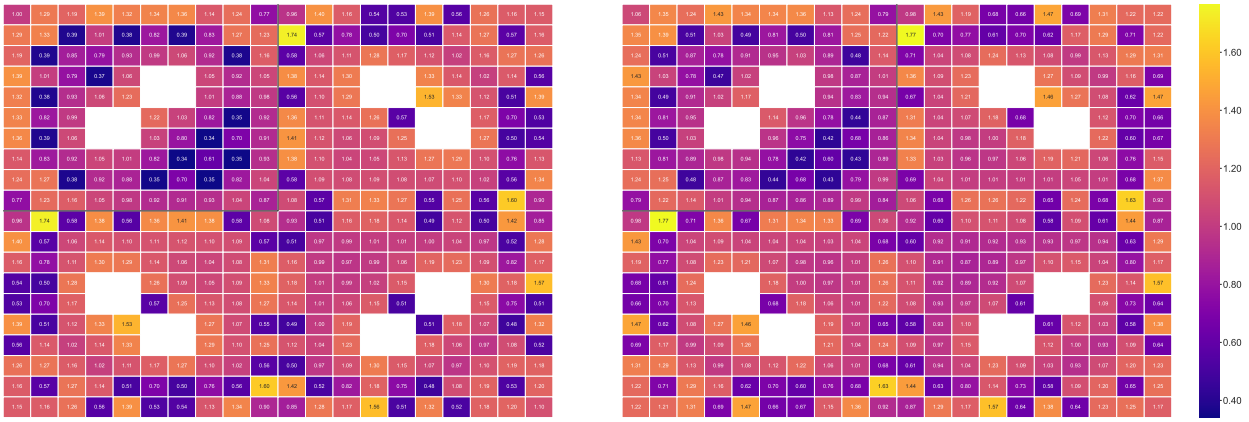

(a) Nominal void (40%) **(b) High void (70%)**

Figure 20. Relative pin power distribution for the Polaris model of the transition core multi-assembly model (LEU and LEU+ assemblies, all fresh) at nominal and high-void conditions.

A notable feature of the pin power peaking factors observed both for the nominal and high-void conditions are the relatively large peaking factors observed near the interface of the LEU and 10.0 $^{w}/_{o}$ ^{235}U maximum LEU+ assembly, representing a region with a relatively high thermal flux gradient between pins, particularly over the inter-assembly gap region. This phenomenon persists for both the fresh and the transition cycle lattices, and it factors prominently into the maximum error in the observed pin power distributions, especially those calculated by PARCS.

4.2.1 NOMINAL VOID CONDITION

Table 12 provides the Polaris/PARCS multi-assembly results for the nominal void lattice (LEU/LEU+ fresh core) case with various few-group structures. The above multi-assembly model assumes all fresh assemblies (i.e., a nominal assembly surrounded by LEU+ assemblies). All errors shown in the table were based on comparisons between the Polaris/PARCS models and the Polaris multi-assembly reference. A high-resolution, CE Monte Carlo calculation using Serpent [5] is used to provide a reference solution to verify the Polaris/PARCS calculation. The Serpent multi-assembly lattice geometry and corresponding Serpent-calculated fission power and flux distribution are illustrated in Figure 21.

Based on Table 12, the Polaris result aligns closely with the Serpent simulation, with small differences in the assembly and pin powers. The k_{eff} difference is below 200 pcm. Compared with the Polaris results, the results from the PARCS calculation have observable differences in k_{eff} , assembly power, and pin powers. The finer (8G) group structure used did not provide a significant improvement over the nodal diffusion calculation. This is because transport effects may be more prominent in the finer group structure; therefore, this finer group structure must be optimized to better improve the results. However, in this case, the 2G result is still acceptable in terms of the error introduced, so this structure was used in the next step of this work.

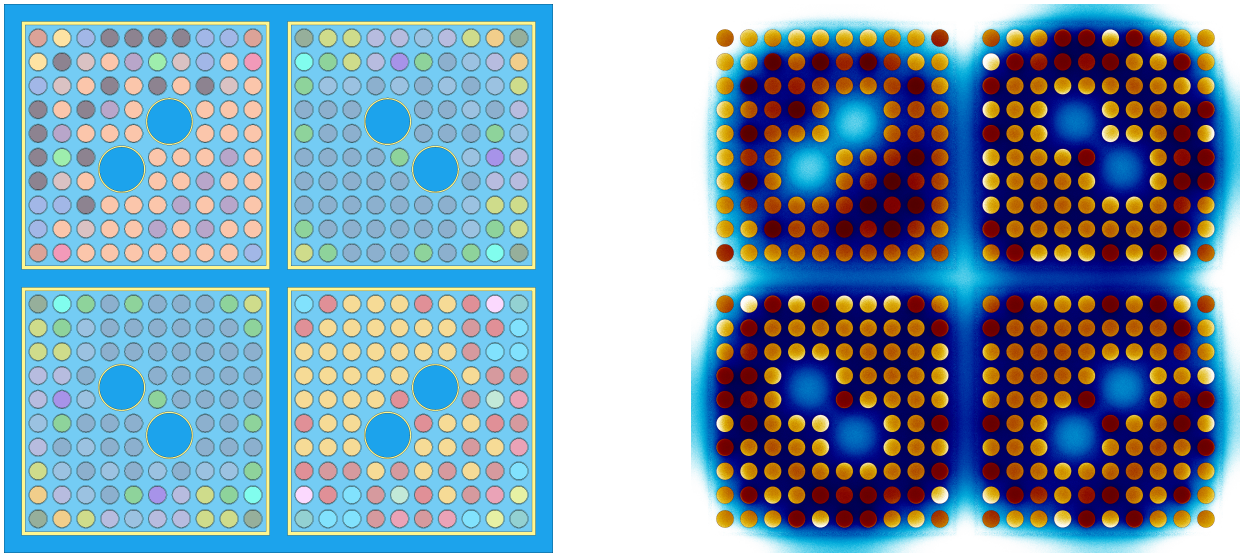

(a) Serpent 2×2 BWR lattice geometry

(b) Serpent relative fission power (red / yellow / orange) and thermal flux distribution (blue)

Figure 21. Serpent BWR 2×2 lattice model and relative power distribution at the beginning of cycle for the LEU/LEU+ mixed core (all fresh assemblies).

Table 12. Relative power distribution and k_{eff} difference for the LEU/LEU+ BWR multi-assembly transition model (all fresh assemblies, LEU surrounded by LEU+) at BOC and nominal void condition for different energy group structures

Model	k_{eff}	Δk_{eff} (pcm)	Difference in relative power (%)			
			Assembly		Pins	
			Average	Max	Average	Max
Polaris (56G)	1.00819	–	–	–	–	–
Serpent (CE)	1.00979 ± 0.00007	186	0.10	0.20	0.42	1.59
PARCS (2G)	1.00942	149	0.89	1.34	0.98	5.24
PARCS (4G)	1.00934	141	0.73	1.24	0.83	4.29
PARCS (8G)	1.00930	137	1.15	1.84	0.88	4.54

The individual pin power errors for the BWR 2×2 assembly model of the transition core (illustrated in Figure 19) are shown as Figure 22. Much like the PWR multi-assembly test (Figure 6), no apparent trend exists in the PARCS group structure selected with respect to the individual pin power errors. The apparent shift in relative power error to the northeast (twice-burned LEU) assembly with an increasing number of energy groups in PARCS is not seen here; rather, the distribution of the relative pin error appears to be relatively fixed. Notably, the Polaris model shows excellent agreement with Serpent in terms of relative pin powers; per Figure 22, the largest differences appear to occur at the assembly interfaces. Moreover, comparing Figure 19 with Figure 21b shows that the largest errors in the PARCS calculations occur in the SE region of the (NW) LEU assembly (i.e., at the interface of the LEU+ assemblies), wherein relatively steep gradients in the pin fission power and assembly thermal flux are observed.

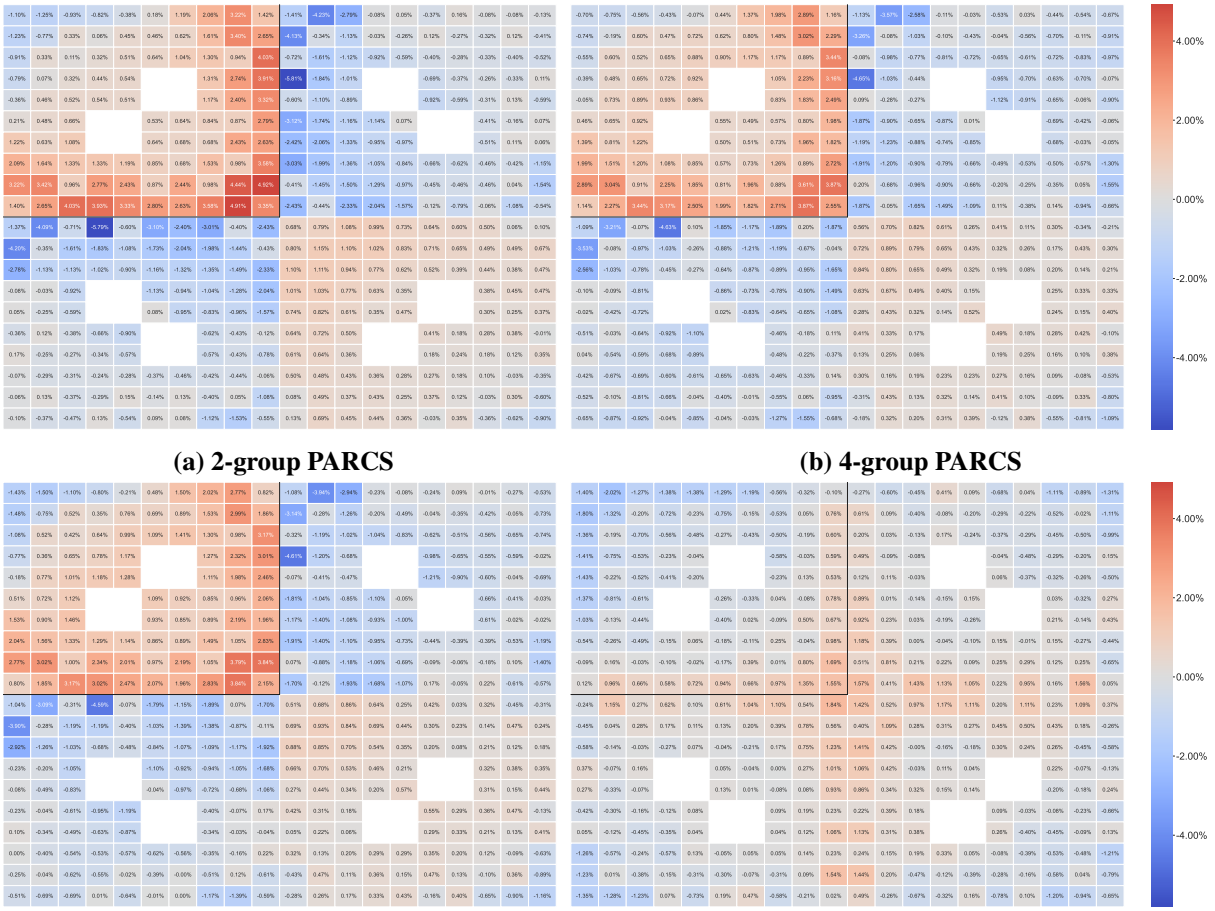

(a) 2-group PARCS **(b) 4-group PARCS**

(c) 8-group PARCS **(d) Serpent (CE)**

Figure 22. Relative pin power differences (beginning of cycle) for the BWR 2×2 supercell for the LEU and LEU+ mixed core (all fresh assemblies) as compared to Polaris for the PARCS few-group models and Serpent CE model.

4.2.2 HIGH-VOID CONDITION

An additional consideration for the BWR case is for a high-void condition (70% void), such as would be experienced by assemblies in the highest-power regions of the core. Applying the same procedure as outlined previously, the power distribution and k_{eff} were evaluated over the transition cycle; the assembly-wise coolant density was modified and set to 70% void (bypass flow outside the channel box

maintained at 0% void). The relative pin powers for the Polaris model of the high-void multi-assembly lattice are illustrated in Figure 20, and the relative errors as compared to Polaris are illustrated for the PARCS 2G, 4G, and 8G models and the Serpent CE model in Figure 23.

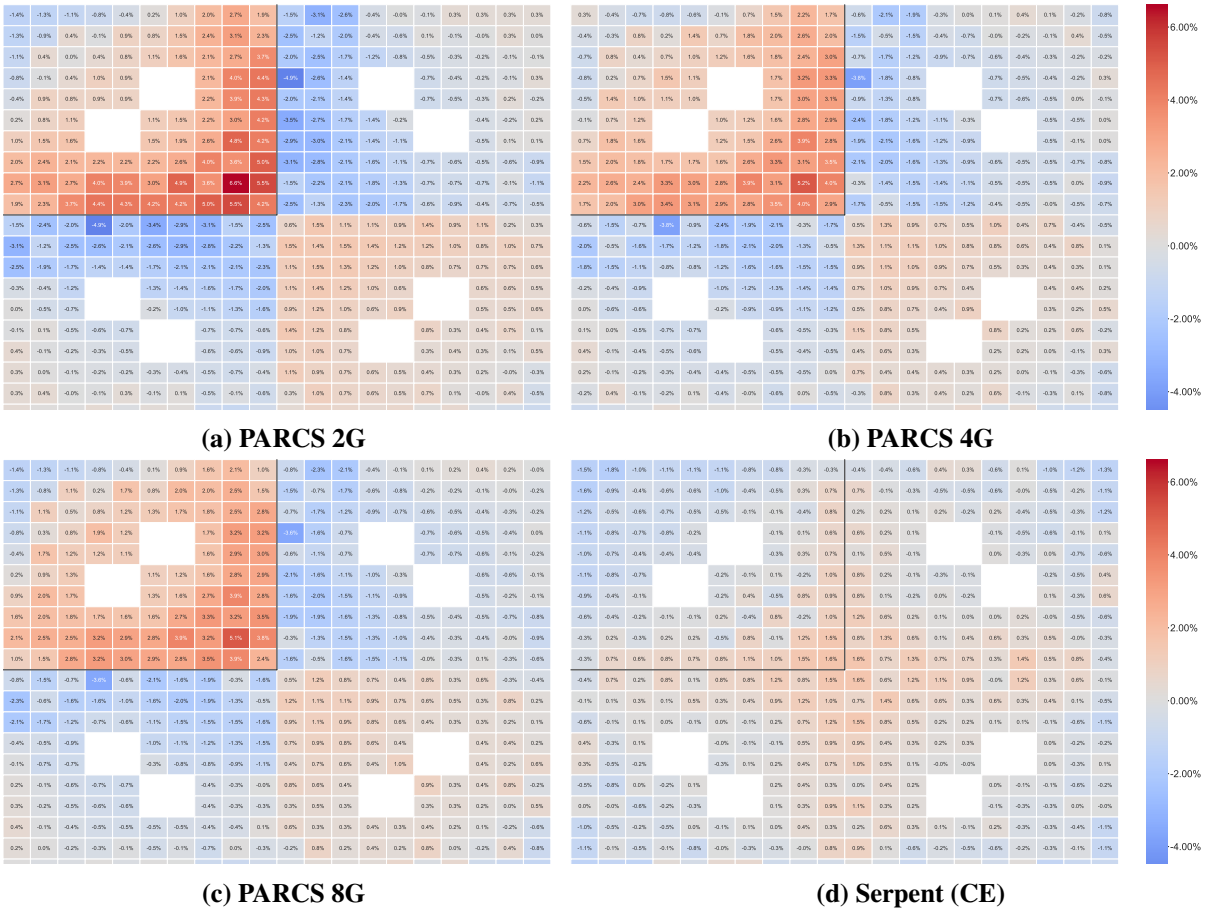

(a) PARCS 2G **(b) PARCS 4G**

(c) PARCS 8G **(d) Serpent (CE)**

Figure 23. Relative pin power differences as compared to Polaris for the high-void transition cycle (LEU and LEU+ multi-assembly model, all fresh assemblies).

In general, the distribution of pin power errors across the multi-assembly lattice changes less than 1% compared to the nominal 40% void condition (Figure 22), indicating that uniform change in the coolant void fraction does not itself introduce any significant source of bias. As before, the errors for the Polaris/PARCS few-group models are clustered around the interface of the LWR assembly with the two 10.0 $^{w}/_{o}$ ^{235}U maximum enrichment LEU+ assemblies, wherein the pin-to-pin peaking gradients are the greatest. This effect is reflected in the overall power distribution of the multi-assembly lattice (Figure 20), wherein the pins with the highest relative power error correspond to regions with the highest pin-to-pin change in PPF.

The overall properties of the error in k_{eff} as well as the assembly and pin power distributions are presented in Table 13. At a global level, the relative errors in the pin and assembly powers largely mirror those of the nominal void case (Table 12). Although the maximum pin power error slightly increases for the PARCS models (by about 1%), the change in void condition does not otherwise appear to result in a significant change in the overall solution accuracy.

Table 13. Relative power distribution and k_{eff} difference for the BWR multi-assembly lattice (all fresh assemblies, LEU surrounded by LEU+) at BOC and high-void condition for different energy group structures

Model	k_{eff}	Δk_{eff} (pcm)	Difference in relative power (%) Assembly Average	Assembly Max	Pins Average	Pins Max
Polaris 2 × 2 (56G)	0.99315	–	–	–	–	–
Serpent 2 × 2 (CE)	0.99303 ± 0.00008	−12	0.10	0.19	0.48	1.76
PARCS (2G)	0.99411	96	1.18	1.73	1.32	6.61
PARCS (4G)	0.99395	80	0.88	1.46	1.01	5.15
PARCS (8G)	0.99390	75	1.41	2.55	1.00	5.11

4.3 LEU-TO-LEU TRANSITION CORE

The next verification step was to test the transition core model using the 2 × 2 assembly lattice in Polaris and PARCS. For the transition core model, the first two cycles consisted of four fresh LEU BWR assemblies with a maximum enrichment of 4.9 w/o ^{235}U and an average enrichment of 4.4 w/o ^{235}U; the reader is directed to Tables 3 and 4 for further details. As before, the LEU-to-LEU transition core comparison provides a baseline performance comparison of the Polaris vs. Polaris/PARCS workflow.

Similar to the PWR transition case, the assumption of a loading of exclusively fresh assemblies is conservative; this is a larger initial reactivity loading than would be realistically observed in practice.

The relative pin powers for the BWR LEU-to-LEU transition core at BOC and EOC are shown as Figure 24. As expected, local power depression is observed in the locations of fresh gadolinia burnable absorber rods in the surrounding assemblies, and the overall power profile flattens toward EOC with higher-power, more reactive assemblies surrounding the depleted LEU assembly.

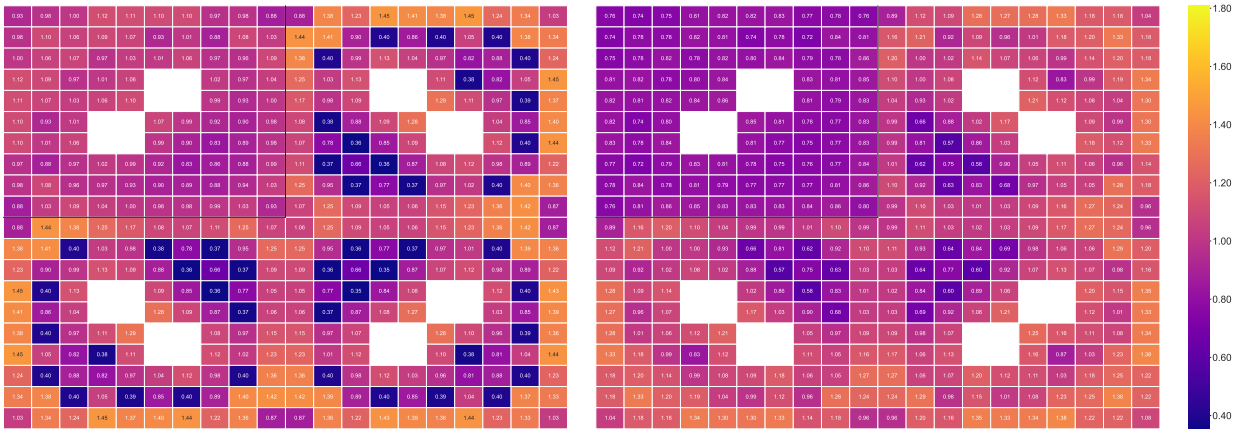

(a) BOC **(b) EOC**

Figure 24. Relative pin power distribution calculated from Polaris for the LEU/LEU+ BWR transition core at BOC and EOC, wherein a twice-burned LEU assembly (NW) is surrounded by fresh LEU assemblies at 8.0 w/o ^{235}U (SE) and 10 w/o ^{235}U (SW and NE).

The relative pin power differences for the LEU-to-LEU core is presented in Figure 25. Overall, the agreement in relative pin powers between Polaris and the Polaris/PARCS calculation is excellent for the

nominal LEU-to-LEU transition core: the differences for most pins are well under 1% at both BOC and EOC.

(a) BOC **(b) EOC**

Figure 25. Relative pin power differences for Polaris/PARCS vs. Polaris for the BWR LEU-to-LEU transition cycle

The assembly power distribution characteristics for the BWR LEU-to-LEU transition core are summarized in Tables 14 and 15. Much like the PWR cases, the Polaris and Polaris/PARCS calculations, overall, show good consistency in terms of both the overall maximum PPF at BOC and EOC as well as the location and magnitude of the peak pin power for the LEU-to-LEU transition core.

Table 14. Characteristics of the BWR LEU-to-LEU transition core (depleted LEU assembly with fresh LEU assembly neighbors) relative to Polaris for the PARCS few-group model.

	Model	k_{eff}	Δk_{eff} (pcm)	Pin PPF	Difference in relative power (%) Assembly Average	Assembly Max	Pins Average	Pins Max
BOC	Polaris 2 × 2 (56G)	1.01259	–	1.451	–	–	–	–
	PARCS (2G)	1.01265	6	1.450	0.07	0.15	0.34	1.31
EOC	Polaris 2 × 2 (56G)	1.06339	–	1.382	–	–	–	–
	PARCS (2G)	1.06425	86	1.375	0.10	0.17	0.36	1.46

4.4 LEU-TO-LEU+ TRANSITION CORE

The second BWR transition core analysis case is that of the transition from an LEU-only core to an LEU+ core. Similar to prior cases, a full LEU multi-assembly lattice is burned for two 20-month cycles at constant power, whereupon in the third cycle, each assembly surrounding the twice-burned LEU assembly is replaced by LEU+ assemblies corresponding to the assembly lattice map in Figure 19.

The relative core power distribution at BOC and EOC, as calculated from Polaris, is shown as Figure 26. As is intuitively expected, at BOC the power peaking is shifted toward the fresh LEU+ / ATF assemblies with comparatively less power produced in the less-reactive twice-burned LEU assembly. Moreover, the power profile across the LEU assembly shows a noticeable tilt: the relative power is significantly lower at the narrow gap, as expected. Local flux depression is clearly seen for the burnable absorber rods in the LEU+ assemblies. At EOC, the power profile is notably flatter: the depletion of the burnable absorbers and

Table 15. Characteristics of power peaking for Polaris vs. Polaris/PARCS calculations for the LEU-to-LEU BWR transition cycle: difference in relative power for the maximum power pin in each model, peak pin location, and the difference in relative pin power at the location of the maximum power pin from Polaris.

	ΔPPF_{max} (%)	Location of peak pin Polaris	PARCS	ΔPPF at max Polaris pin (%)
BOC	−0.14	(1,17)	(1,17)	−0.14
EOC	−0.76	(1,17)	(1,17)	−0.14

similar power tilt are observed across wide–wide and narrow–narrow gaps. Meanwhile, the power profile in the LEU assembly is far more uniform than at BOC.

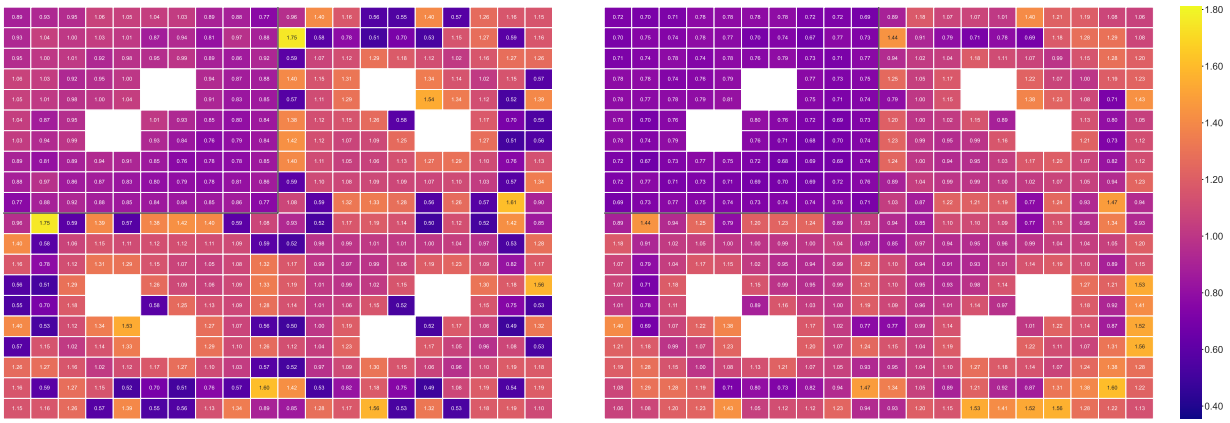

(a) BOC **(b) EOC**

Figure 26. Relative pin power distribution calculated from Polaris for the BWR transition core at BOC and EOC, wherein a twice-burned LEU assembly (NW) is surrounded by fresh LEU+ assemblies at 8 w/o ^{235}**U (SE) and** 10 w/o ^{235}**U (SW and NE).**

The relative pin power differences at BOC and EOC for the LEU-to-LEU+ transition core is shown in Figure 27. Notably, the relative pin power differences at the interface between the (twice-burned) LEU assembly and the fresh LEU+ assemblies at BOC are considerably higher than those of the LEU-to-LEU transition core. On both assembly faces at the LEU+ interfaces, the Polaris/PARCS calculation overestimates pin powers in the LEU assembly, with a corresponding underestimate of powers in nearby pins of the adjacent LEU+ assemblies. By contrast, the pin power errors in the non-adjacent 8 w/o ^{235}U assembly (SE quadrant) shows relatively small errors at BOC, indicating that the problem is at the interface of the twice-burned and fresh assemblies.

Of note is that the largest errors in the 10 w/o ^{235}U LEU+ assemblies occur at 10 w/o ^{235}U and 8 w/o ^{235}U pins, respectively, located at the edge of the LEU+ assembly. These regions represent the highest pin-to-pin peaking gradients (i.e., fresh 8 w/o ^{235}U and 10 w/o ^{235}U pins across from depleted 3.9 w/o ^{235}U and 4.9 w/o ^{235}U pins). As seen in the fresh multi-assembly energy group study (Figures 22 and 23), the bias pattern observed at BOC is similar to that observed for the all-fresh assembly lattice. Although such pin-to-pin gradients are observed elsewhere within the assemblies, here the gradient occurs across the inter-assembly gap, resulting in a substantially more thermalized neutron population (see Figure 21b). This strongly suggests that the combination of the pin-to-pin gradient located across the inter-assembly gap is

the cause of the observed biases in this region.

(a) BOC **(b) EOC**

Figure 27. Relative pin power differences for Polaris/PARCS vs. Polaris for the BWR LEU-to-LEU+ transition cycle.

This trend is similarly evident but more subdued at the EOC state, wherein the pin power overestimates in the LEU assembly are generally smaller (in the range of 1–2.8%) as are the under-estimates of pin powers at the LEU assembly interfaces (decreasing from to a maximum of −9.1% at BOC compared to −7.5% at EOC). Once again referring back to the thermal flux distribution in Figure 21b, this appears to be the result of the relatively higher thermal neutron population at the inter-assembly gap region introducing a greater sensitivity to the pin-to-pin gradients across the gap region.

The assembly power peaking characteristics for the BWR LEU-to-LEU+ transition cycle are summarized in Tables 16 and 17. Compared to the LEU-to-LEU BWR transition cycle and corresponding PWR cases, the power distribution shows elevated errors between Polaris and Polaris/PARCS. Although the location of the peak pin is consistent between the two models, the peak power at the maximum power pin location and the overall pin PPFs are significantly under-predicted by Polaris/PARCS at the BOC; this is evident in the rather large difference between the maximum PPF observed between Polaris and Polaris/PARCS. This difference, however, appears to dissipate at the EOC, at which point the difference in peak pin powers is considerably smaller.

Table 16. Characteristics of the BWR LEU-to-LEU+ transition core (depleted LEU assembly surrounded by fresh LEU+ assemblies) as compared to Polaris for the PARCS few-group model.

					Difference in relative power (%)			
					Assembly		Pins	
	Model	k_{eff}	Δk_{eff} (pcm)	Pin PPF	Average	Max	Average	Max
BOC	Polaris 2 × 2 (56G)	1.02324	–	1.748	–	–	–	–
	PARCS (2G)	1.02407	83	1.599	0.79	1.16	1.02	9.06
EOC	Polaris 2 × 2 (56G)	1.07195	–	1.506	–	–	–	–
	PARCS (2G)	1.07209	14	1.590	0.41	0.66	0.99	7.52

In order to further determine the causes of the pin power discrepancies near the assembly interface regions, a modified 10 w/o ^{235}U lattice was constructed which the gadolinum-bearing pins are removed from the

Table 17. Characteristics of power peaking for Polaris vs. Polaris/PARCS calculations for the LEU-to-LEU+ BWR transition cycle: difference in relative power for the maximum power pin in each model, peak pin location, and the difference in relative pin power at the location of the maximum power pin from Polaris.

	ΔPPF_{max} (%)	Location of peak pin Polaris	PARCS	ΔPPF at max Polaris pin (%)
BOC	−6.86	(2,11)	(2,11)	−6.86
EOC	−0.94	(19,19)	(19,19)	−0.94

outermost row (i.e., at the assembly interface); the row of 10 w/o ^{235}U pins (both those with gadolinium and those without) are replaced by 8.0 w/o ^{235}U and 9.0 w/o ^{235}U enrichment pins in order to reduce the strong reactivity gradient across the interface; maps of the modified assembly are given as Figure 28.

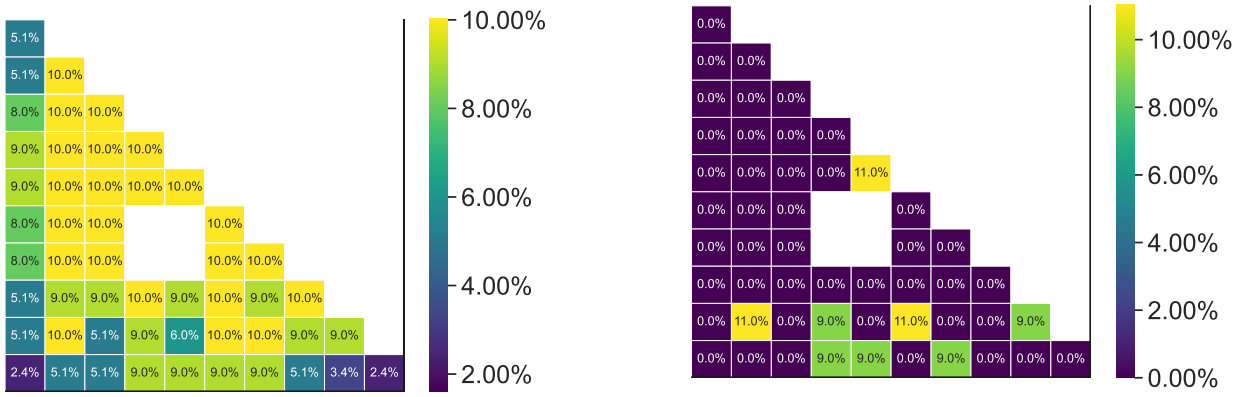

(a) Uranium enrichment **(b) Gadolinia concentrations**

Figure 28. Pin enrichments and gadolinia concentration (wt. %) for the modified 10 w/o ^{235}U maximum enrichment LEU+ assembly used to isolate the cause of large observed pin power discrepancies at the assembly interfaces.

The pin power comparison was subsequently re-examined for this modified map, the results of which are shown as Figure 29. One immediately notices that in contrast with the unmodified assembly with Gd-bearing pins at the interface (Figure 27), PARCS no longer under-predicts pin powers for the 10 w/o ^{235}U lattices at the assembly interface region with the depleted LEU assembly. Rather, PARCS moderately over-predicts pin powers in this region proportional to the individual pin enrichments, with the highest errors occurring in the 9.0 w/o ^{235}U pins at the 10 w/o ^{235}U LEU+ assembly interfaces.

The results of this modified lattice investigation would suggest that the large relative errors in pin powers observed at the interfaces in Figure 27 arise from limitations in how pin power peaking factor information is conveyed to PARCS in multi-assembly calculations using cross-sections generated using Polaris. Specifically, PARCS relies upon cross-sections generated using a single reflected assembly for each assembly within the core, applying assembly disadvantage factor (ADF) correction factors to account for interface effects between assemblies. However, because the 1×1 pin power maps inherently do not capture strong gradients at the interface arising from features such as high-enrichment pins adjacent to depleted pins in an adjacent assembly, the initial pin power maps derived from Polaris 1×1 calculations are too far off from the actual solution for the PARCS solver to correctly converge upon pin powers for these regions.

This is made evident by the observed behavior of when the Gd pins are removed from the assembly interfaces and a smooth enrichment gradient is introduced; instead of observing very large, localized power under-predictions between the Gd rods, instead a more moderate but continuous pattern of power over-prediction is instead observed in this region.

This experiment would thus appear to indicate a condition where users need to be especially cautious with multi-assembly calculations using Polaris with PARCS to ensure that cross-sections generated for individual assemblies accurately capture neighbor effects such as large reactivity gradients across the assembly interface. Specifically, this study finds that the largest pin power errors are associated with the pins with the largest change in reactivity to their corresponding neighbors in the adjacent assembly.

4.5 LEU-TO-ATF CORE

The relative pin power differences at BOC and EOC for the LEU-to-ATF transition core is shown in Figure 31.

Table 18 provides an overview of the differences in assembly and pin powers for the Polaris and Polaris/PARCS model of the LEU-to-ATF transition cycle.

For the ATF transition core, there is a moderate over-estimation of the assembly power by PARCS in the twice-burned LEU assembly (NW), with errors ranging from about -1.3 to 4.4% at BOC and -1.9 to 3.3% at EOC. The largest discrepancies in pin powers again appear at the LEU / ATF interfaces, consistent with the behavior of the LEU / LEU+ lattice, with a maximum underestimation of -11.4% at BOC.

Table 18. Characteristics of the BWR LEU-to-ATF transition core (depleted LEU assembly with fresh ATF assembly neighbors) relative to Polaris for the PARCS few-group model.

	Model	k_{eff}	Δk_{eff} (pcm)	Pin PPF	Difference in relative power (%) Assembly Average	Assembly Max	Pins Average	Pins Max
BOC	Polaris 2 × 2 (56G)	1.01562	–	1.808	–	–	–	–
	PARCS (2G)	1.01665	103	1.719	0.07	0.15	1.17	11.44
EOC	Polaris 2 × 2 (56G)	1.03964	–	1.532	–	–	–	–
	PARCS (2G)	1.03917	−47	1.546	0.10	0.17	1.12	8.88

Table 19 provides a further breakdown of the overall peak power distribution for the LEU-to-ATF core. Though the maximum difference in PPF at BOC is smaller compared to the LEU-to-LEU+, the PPFs do not appear to converge over the cycle, unlike prior transition cycle calculations. The location of the peak pin location is again consistent between Polaris and Polaris/PARCS, although the nontrivial difference in magnitude is again indicative of the large differences in the power distribution between the two calculations.

The general pattern of discrepancies near the assembly interface region appears to continue a trend first observed in the BWR LEU-to-LEU+ core at BOC, seen previous in Figures 26 and 27. Here, the introduction of LEU+ assemblies results in nontrivial errors in calculated pin powers at the interface of the LEU/LEU+ assemblies. In both cases, an underestimation in the pin powers near the interface region appears to be counter-balanced by a moderate over-estimation of pin powers in the twice-burned LEU assembly (NW corner).

Finally, due to the non-uniform nature of the lattices for the BWR LEU / ATF transition core (wherein compensate for the parasitic capture effects of the FeCrAl cladding, the pin radius of the ATF assemblies

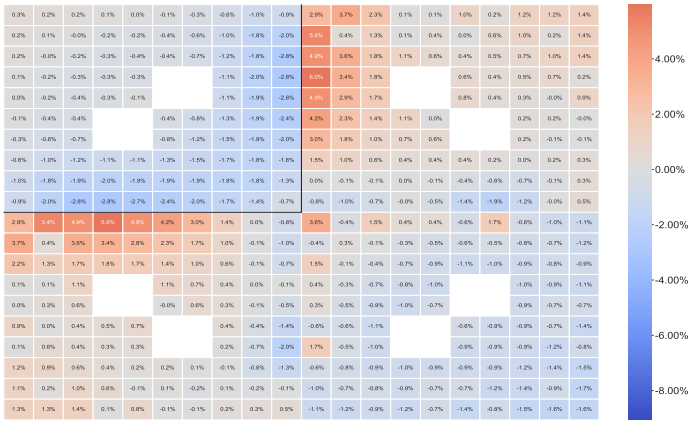

Figure 29. Relative pin power differences at BOC for Polaris/PARCS vs. Polaris for the BWR LEU-to-LEU+ transition cycle employing a modified LEU+ lattice.

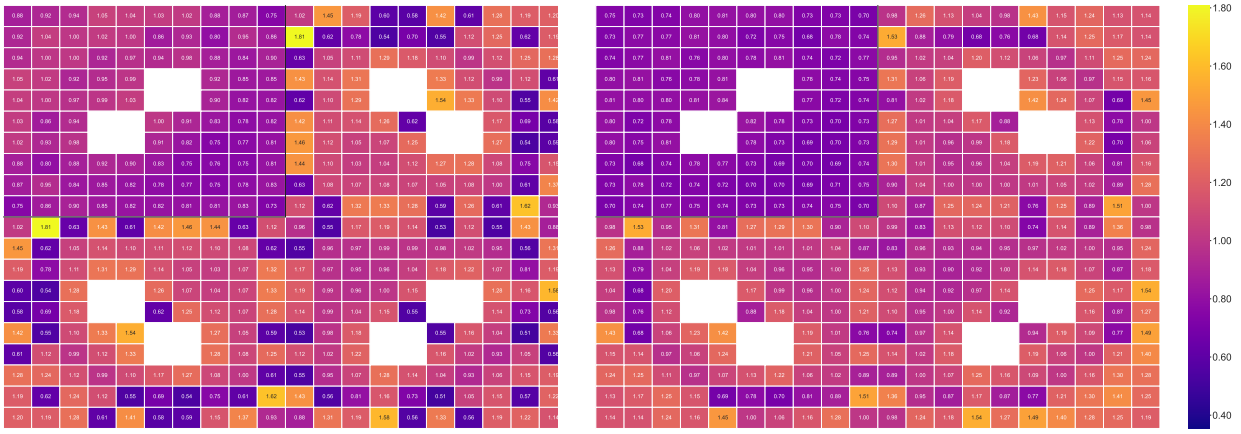

(a) BOC **(b) EOC**

Figure 30. Relative pin power distribution calculated from Polaris for the BWR transition core at BOC and EOC, wherein a twice-burned LEU assembly (NW) is surrounded by fresh ATF assemblies at 8.0 w/o ^{235}U (SE) and 10 w/o ^{235}U (SW and NE).

(a) BOC **(b) EOC**

Figure 31. Differences in relative pin power for Polaris/PARCS vs. Polaris for the BWR LEU-to-ATF transition cycle

Table 19. Characteristics of power peaking for Polaris vs. Polaris/PARCS calculations for the LEU-to-ATF BWR transition cycle: difference in relative power for the maximum power pin in each model, peak pin location, and the difference in relative pin power at the location of the maximum power pin from Polaris.

	ΔPPF_{max} (%)	Location of peak pin Polaris	PARCS	ΔPPF at max Polaris pin (%)
BOC	−8.93	(2,11)	(2,11)	−8.93
EOC	0.13	(2,11)	(2,11)	−8.93

increases by 0.0285 cm, resulting in a heavy metal mass gain of 13.4% per pin), the pin power factor edits reported by Polaris needed to be renormalized in order to correctly compare pin power peaking factors between PARCS and Polaris. Specifically, PARCS uses the following definition for the form function $f_g(x,y)$ [3]:

$$f_g(x,y) = \frac{\kappa\Sigma_{f,g}(x,y)\,\phi_g(x,y)}{\kappa\overline{\Sigma}_{f,g}\overline{\phi}_g} \tag{1}$$

Thus the pin powers derived from Eq. (1) are:

$$p(x,y) = \sum_{g=1}^{G} \kappa\overline{\Sigma}_{f,g}\phi_g(x,y)\,f_g(x,y) \tag{2}$$

The pin power factors produced by Polaris thus effectively provide *volumetric* heat generation shape factors. When dealing with a lattice geometry with homogeneous pin geometries, this is thus equivalent to the pin power shape function. However, in the LEU-ATF transition core case, this is no longer true and thus the pin power factors must be correctly normalized to account for the differences in pin geometry.

Normalization was thus performed by scaling the pin power factors within each quadrant by the ratio of the volume of pins within a given quadrant to the problem-averaged pin volume, i.e.:

$$p'(x,y) = p(x,y)\cdot\frac{r_{x,y}^2}{\overline{r}^2} \tag{3}$$

Making this correction is required for the LEU/ATF case in order to calculate the correct pin powers for each assembly in the 2×2 lattice.

Note that this correction only needed to be applied to the BWR supercell due to the change in fuel pin geometry between LEU and ATF designs (see Table 3); because the pin dimensions for the PWR case are unchanged for the ATF design, this correction was not necessary there.

4.6 REACTIVITY ANALYSIS OF THE BWR MULTI-ASSEMBLY TRANSITION CYCLES

With the overall distribution of assembly and pin powers characterized between the two calculations for each of the BWR transition cycles, the next part of this analysis is to compare reactivity effects between these models—specifically, comparing k_{eff} and reactivity coefficients such as CBW and DTC. This comparison for k_{eff} over each cycle is shown in Figure 32. Notably, k_{eff} increases over the first cycle,

leveling out and slightly decreasing over the second cycle, corresponding to the depletion of the gadolinium-bearing rods. For each scenario, k_{eff} is expected to be identical for the first two cycles (i.e., up to 1200 days), given that these cycles are exclusively composed of LEU fuel.

Overall, the calculations produce excellent agreement for k_{eff} (i.e., within ±100 pcm), with the LEU-to-LEU cycle showing the tightest overall agreement (within ±50 pcm). Note that the CBW cannot be feasibly modeled with a multi-assembly model using Polaris because of the way the system is modeled using Polaris. Within Polaris, the control blade geometry is defined with respect to the northern wing (which is then reflected to the western wing), effectively assuming a single-assembly model with the control blade inserted at the wide-wide corner [1]. As such, it is not possible to model control blade insertion for a multi-assembly model, as this would require placement of the control blade at the center of the multi-assembly model.

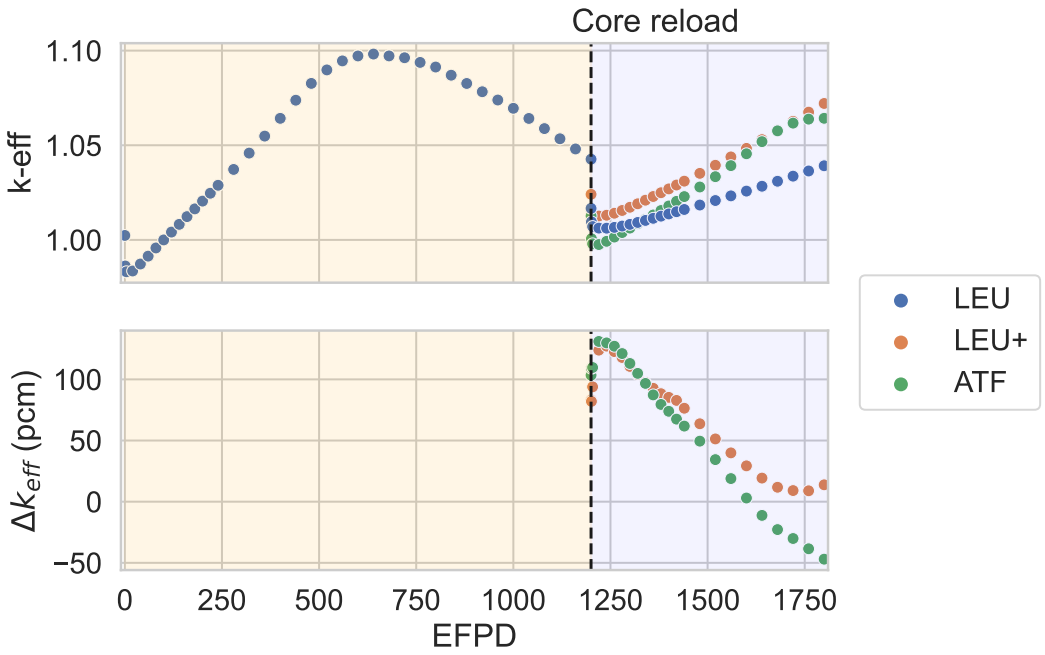

Figure 32. k_{eff} comparison for transition models for BWR multi-assembly model compared between Polaris and PARCS for each burnup step; cycle boundaries occur at 600 and 1200 EFPD, with the transition core reload occurring at 1200 EFPD. Shaded regions indicate (light orange) nominal core loading and (light blue) twice-burned LEU assemblies surrounded by three LEU+ assemblies.

The DTC for the BWR 2 × 2 supercell transition cycle is shown for each of the three transition cores evaluated in Figure 33. Here, the change to LEU+ fuel results in a reduction of DTC of about −6 to −10%, with the difference generally growing over the length of the cycle. The ATF core shows a similar trend, showing very similar burnup dependence as the LEU+ assemblies, although with an overall smaller effect on DTC, ranging from about −2 to −8% compared to the nominal LEU transition core.

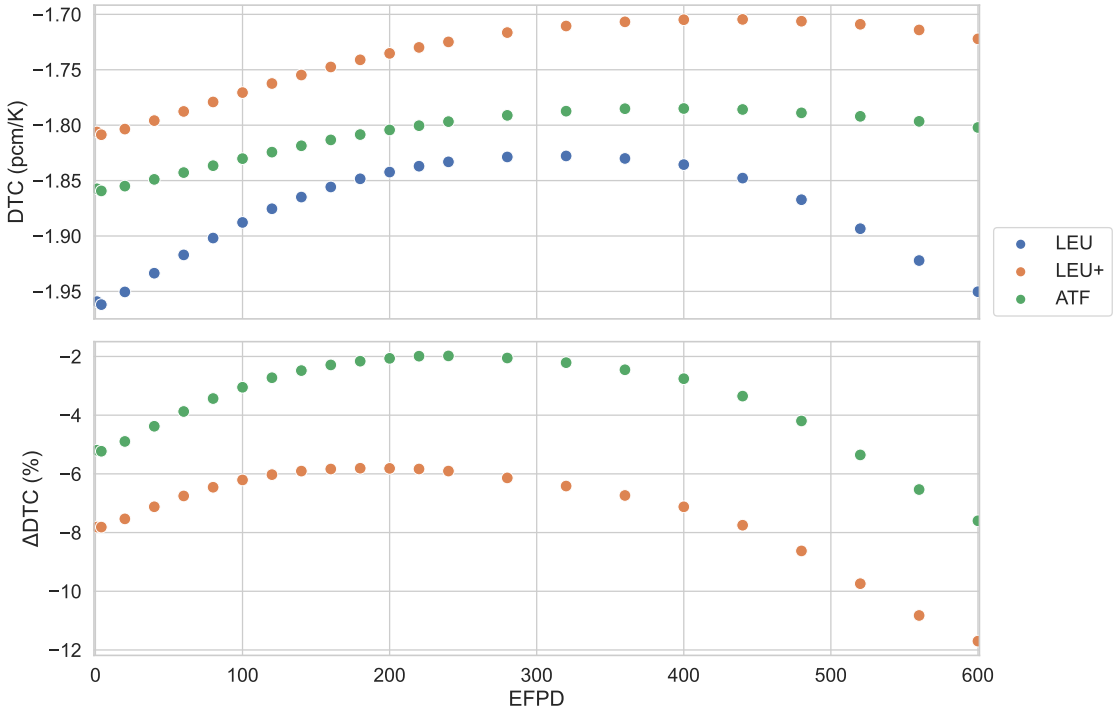

Figure 33. (top) Doppler temperature coefficient (DTC) for the Polaris BWR 2×2 assembly model transition cycle for the LEU-to-LEU, LEU-to-LEU+, and LEU-to-ATF/LEU+) assemblies (bottom) Difference in DTC relative to the LEU-to-LEU transition core.

5. BWR FULL-CORE TRANSITION CYCLE CALCULATION

The calculation procedures verified in Section 4 for multi-assembly models can be used to simulate the transition calculation for the whole-core model. This section thus focuses on evaluating the relative change in key reactor quantities such as the DTC and CBW relative to the LEU-only core for the LEU-to-LEU+ and LEU-to-ATF cores. In addition, the relative power distribution at BOC and EOC is compared for each of these three conditions (LEU-to-LEU, LEU-to-LEU+, and LEU-to-ATF transition cores).

5.1 POLARIS/PARCS BWR WHOLE-CORE MODEL

The core model used is based on the geometry and size of the Edwin I. Hatch reactor core [4], [16], [17] and adapted from a parallel effort on generating BWR equilibrium cores for Phase II studies [18]. Figure 34 presents the quarter-core map of the reactor model used. The loading pattern for this core is designed for 36-month cycle LEU+ fuel.

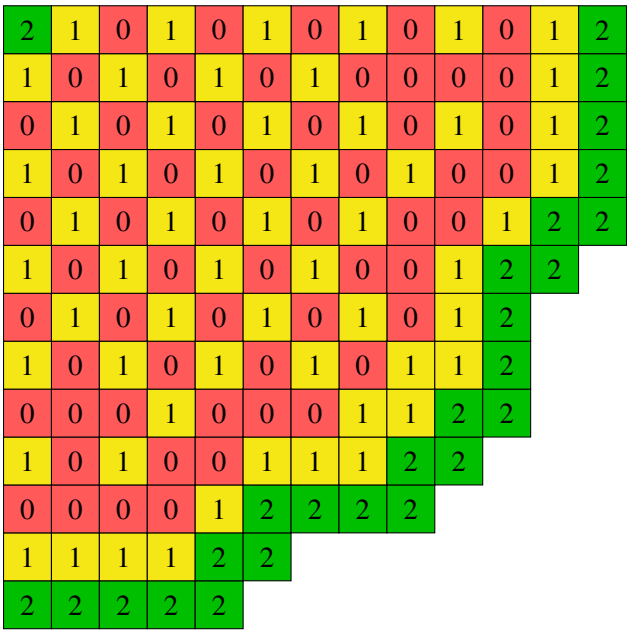

Figure 34. Quarter-core map of a BWR core with three cycles of fuel loading, modeled in PARCS. The numbering (and cell colors) represent the number of previous irradiation cycles for each fuel assembly.

The multi-cycle calculation was performed in PARCS to handle the fuel shuffling and loading in the core model. Each cycle includes an 20-month reactor operation with 720 days of full reactor power operation at 30 $\frac{\text{MW}}{\text{MTU}}$, an average void fraction of 40% (corresponding to a moderator density of 0.4578 $\frac{\text{g}}{\text{cm}^3}$), a fuel temperature of 950 K, and a moderator temperature of 560 K. Thermal hydraulic reactivity effects as well as xenon and samarium feedbacks were explicitly accounted for. Using this approach, a transition core can be modeled by replacing the fresh batch of the fuel with fresh LEU+ and ATF assemblies. In this work, three different core simulations were conducted in PARCS.

1. LEU-to-LEU core, which includes the standard 4.9 $^{\text{w}}/_{\text{o}}$ ^{235}U maximum with Zircaloy-2 cladding fuel assemblies.

2. LEU-to-LEU+ transition core, which replaces some fuel assemblies in the core on the third cycle with the 10.0 $^{w}/_{o}$ ^{235}U maximum fuels and Zircaloy-2 cladding fuel assemblies.
3. LEU-to-ATF transition core, which replaces some fuel assemblies on the third cycle with the 10.0 $^{w}/_{o}$ ^{235}U maximum assemblies with FeCrAl cladding.

Note that in each transition core scenario, *all* of the LEU fuel that would be shuffled out of the core is replaced with the LEU+ / ATF assemblies; that is, the new assembly types are loaded in the once-burned positions indicated in Figure 34. This, of course, is a far more aggressive reloading approach than would be conventionally applied in a commercial reactor in which the transition would occur more gradually. Likewise, the introduction of fuel with a different reactivity curve would necessitate introduction of an alternative core loading pattern so as to maintain power peaking factors throughout the core. However, the intent of this analysis is not to attempt to produce an optimized core loading pattern; rather, the goal is to present a limiting case, that is, evaluating the most extreme scenario to bound factors such as PPFs, DTC, and CBW.

5.2 CORE POWER DISTRIBUTIONS

One of the most interesting parameters to compare in this case is the power distribution in the reactor. The assembly power is calculated as the fission energy generation rate per fission (from the Polaris transport calculation), which is then multiplied by the (multigroup) neutron scalar flux and the node volume, then summed for all energy groups. In PARCS, the power distribution is normalized so that the average core power across all assemblies is unity.

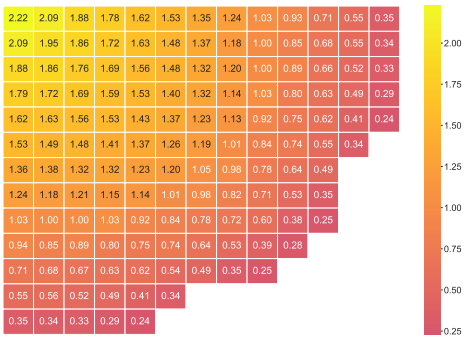

(a) LEU-to-LEU transition core

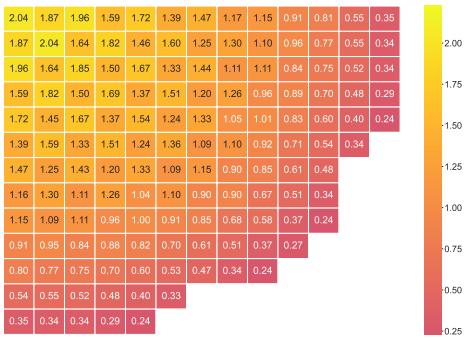

(b) LEU-to-LEU+ transition core

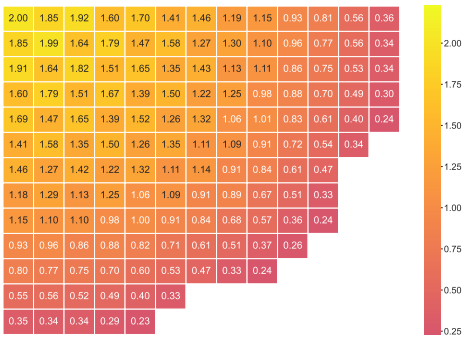

(c) LEU-to-ATF transition core

Figure 35. BOC relative core power distribution for LEU-only, extended enrichment (LEU+), and ATF with extended enrichment core loadings.

Figure 35 presents the core power distribution at BOC for the three reactor cores. In general, the assembly power distribution for LEU, LEU+, and ATF cores show similar spatial trends. Notably, higher reactivity

in LEU+ and ATF assemblies reduce the central peaking, whereas a more distinctive checkerboard power pattern is visible due to their higher reactivity compared to the LEU assemblies.

At EOC, the checkerboard loading pattern becomes even more visible for the new fuel types, whereas the LEU core, in contrast, exhibits a smooth gradient. This power shape is expected as LEU+ and ATF cores are designed for 36-month cycles and still have higher reactivity at the end of their 24-month cycles. Figure 36 and Table 20 summarize these values. Notable among these distributions is that the BOC radial assembly power is lower in comparison to the LEU+ and ATF cores as a result of higher reactivity from the fresh fuel zone at the periphery. A small increase in peak assembly power is observed in these cores compared to the transition LEU core. As expected, all cores show the power shift toward the periphery at EOC, again because of the fresh fuel zone in this core design.

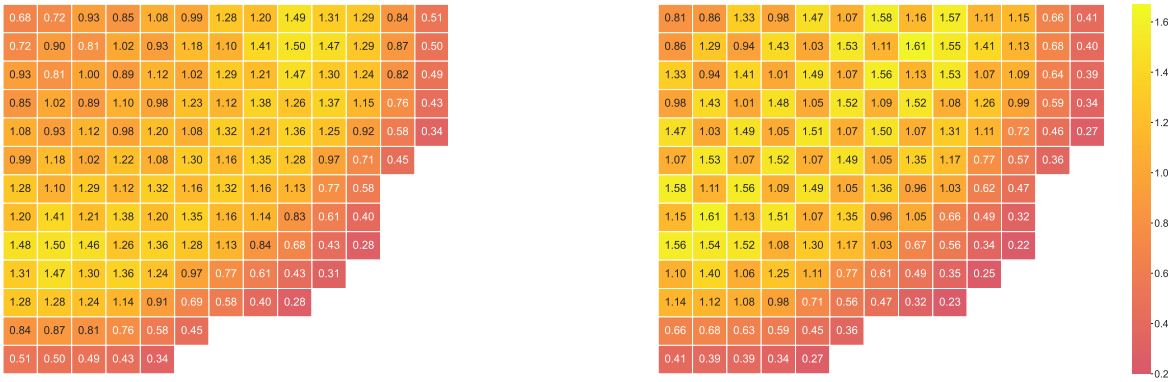

(a) LEU-to-LEU transition core

(b) LEU-to-LEU+ transition core

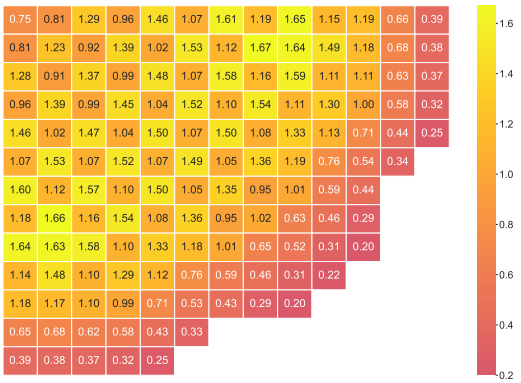

(c) LEU-to-ATF transition core

Figure 36. EOC relative core power distribution for LEU-only, extended enrichment (LEU+), and ATF with extended enrichment core loadings.

Table 20. Radial assembly power peaking factors at BOC and EOC for the BWR full-core transition cycles.

Transition core	BOC	EOC
LEU-to-LEU	2.22	1.50
LEU-to-LEU+	2.00	1.67
LEU-to-ATF	2.04	1.61

5.3 REACTIVITY COEFFICIENTS AND CONTROL BLADE WORTH

Reactivity coefficients and CBW are important parameters in reactor safety analysis. In this work, DTC and CBW are compared for the three core models in Figures 37 and 38. For each core, the DTC decreases until around 100 days (corresponding to the point of peak reactivity in the cycle); from this point on, the DTC monotonically increases in magnitude throughout the rest of the cycle. Notably, the relative difference in the LEU+ and ATF cores (as compared to LEU) shows nearly identical behavior patterns in terms of the relative difference in DTC, differing only in relative magnitude. This indicates that the effect of higher assembly enrichment dominates the effect on DTC, with parasitic capture effects in the ATF cladding partially mitigating this effect. The trend in DTC with burnup and difference in magnitude for each fuel type is consistent with the trends and magnitudes observed in multi-assembly study in Section 4 and in the Phase I studies [6], [8].

In general, the relative differences between the LEU+ and ATF cores are moderate compared to the LEU-only transition cores, with differences for the LEU+ transition core ranging from −4.79% at BOC to −7.55% at EOC and from −3.06% at BOC to −5.73% at EOC for the LEU+/ATF core.

This result is in line with the previous assembly-level calculations that FeCrAl-clad fuel assemblies with larger fuel pellets have slightly higher CBWs and DTCs [8]. On the other hand, the introduction of higher-enrichment fuels in the ATF transition core made the CBW and DTC significantly smaller than the LEU and ATF transition cores. This is also in agreement with the previous work on the extended enrichment fuel assemblies [6], [8].

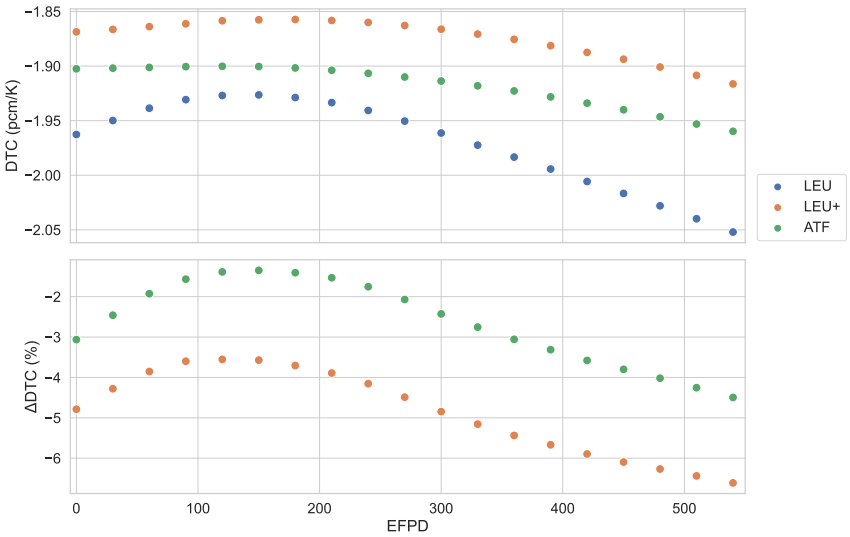

Figure 37. DTCs and relative difference to the LEU core (ΔDTC) for the BWR full-core model over the 20-month transition cycle for the LEU-to-LEU, LEU-to-LEU+, and LEU-to-ATF cores, assuming 10 w/o ^{235}U enrichment for LEU+ / ATF assemblies.

Figure 38 shows the evolution of the CBW for the BWR full-core model over the 20-month transition cycle. Both the LEU+ and ATF transition cores defined in the Phase I study [6] show a substantial decrease in the CBW relative to the LEU transition core (about 5000–7000 pcm, for a relative difference in the range of 20–28%). In all cases, the CBW increases with burnup over the transition cycle; however, a notable feature is the relatively lower rate of increase in CBW over time for the ATF core as compared to LEU+ variant. This effect can be observed in terms of the absolute CRW (Figure 38, top) and more clearly in the behavior of the relative difference in CBW for LEU+ and ATF (Figure 38, bottom). Notably, design

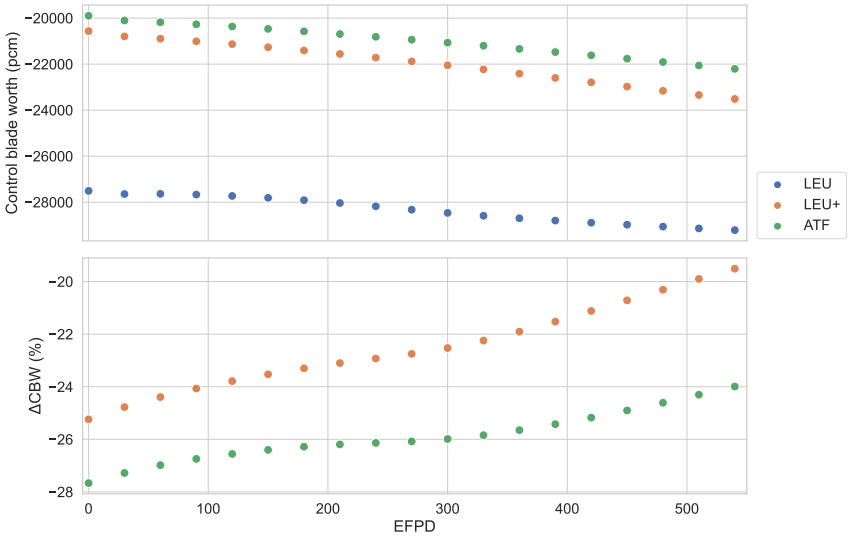

Figure 38. CBW and relative difference to the LEU core (ΔCBW) for the BWR full-core 20-month cycle model for the LEU-to-LEU, LEU-to-LEU+, and LEU-to-ATF cores over the 20-month transition cycle, assuming 10 w/o ^{235}**U LEU+ / ATF assemblies.**

changes to the ATF fuel (such as the larger fuel pellet diameter designed to offset parasitic capture effects by the FeCrAl cladding) drive the observed decrease in CBW relative to its LEU+ counterpart.

6. CONCLUSIONS

Challenging fuel assembly combinations that can be encountered in a transition cycle of LEU+ and ATF in LWRs were simulated in multi-assembly (PWR and BWR) and core (BWR only) models using a Polaris/PARCS two-step calculation procedure. Polaris supercell models were used as reference solutions in all transition cycle multi-assembly assessments. Core physics quantities of interest—such as eigenvalue, power distribution, control rod worth, and Doppler temperature coefficients—are compared between different transition models to understand the impact of introducing advanced fuels in transition cycles. Each Polaris/PARCS model was evaluated for nominal (no new fuel type transition), LEU+, and ATF with LEU+ enrichments. In addition to core physics parameters, the effect of the number of groups in the few-group cross section sets was investigated in the fresh fuel multi-assembly benchmarks. For each case, a corresponding Serpent CE calculation was performed to provide a reference result for both the Polaris MG and Polaris/PARCS FG models. All investigated core parameters strongly depend on fuel assembly and core design; therefore, this study aimed to highlight values for challenging designs.

The results of the PWR and BWR multi-assembly models and BWR full-core model can be summarized as follows.

1. The PWR multi-assembly configuration with a fresh LEU assembly surrounded by ATF assemblies shows excellent agreement among Polaris, PARCS, and Serpent codes in eigenvalue and assembly power comparisons. Pin power differences are the highest around the LEU–ATF interface, reaching 2.3%. An increasing number of energy groups in few-group cross sections yields no consistent improvements in the results. A similar configuration for a BWR multi-assembly lattice shows constant bias in eigenvalue (~150 pcm), maximum assembly power (~1.3%), and maximum pin power difference (~4.29–5.24%) across all different few-group cross section libraries. BWR pin powers also exhibit the largest discrepancies around the LEU assembly interface. Increasing the void fraction to 70% from the nominal 40% does not affect the differences significantly. This study concludes that more detailed investigation regarding the few-group cross sections' energy group boundaries should be performed for optimized results.
2. For PWR multi-assembly transition cycle analysis, Polaris multi-assembly models and PARCS results agree within 50 pcm in k_{eff} throughout the cycle, and no significant change in peak pin power differences was observed between the LEU-only, LEU+, and ATF fuel cycles. Although the BWR multi-assembly transition cycle analysis shows similar differences in k_{eff} (less than 90 pcm) and assembly power predictions between Polaris and PARCS simulations for the nominal and LEU+ cycles, the LEU+ transition cycle can have up to a 6% difference in individual pin powers compared to the nominal LEU cycle. Considering that the largest differences are observed at high pin power locations next to the assembly gap between LEU–LEU+ fuel, the increased error in pin power predictions is believed to be a result of steep flux gradients exacerbated by non-optimal lattice designs. This behavior was also observed in the fresh multi-assembly calculations at a reduced level. The BWR core calculations do not show the large pin peaking factors observed in multi-assembly models due to high-burnup LEU fuel being at the low power core periphery. Therefore, the observed discrepancies in powers are expected to be lower or not an issue because of their relative power in full-core analysis. However, further assessment of the PARCS pin power reconstruction capabilities for challenging multi-assembly problems is recommended.
3. In PWR and BWR multi-assembly models, the transition to LEU+ and ATF designs results in a reduction of the DTC consistent with Phase I study results. Although a decrease of less than 2% was observed at peak reactivity, the difference can be as high as 12% toward end of the cycle. A large

portion of this difference is due to the fact that as the reactivity of LEU decreases, LEU+ and ATF fuel stay highly reactive and do not experience the same increase in DTC at EOC as the LEU fuel. This effect is much less pronounced in full core (BWR only), with the differences dropping below 6% at EOC. For all cases, ATF exhibits less or identical differences with the LEU+ fuel.

4. Similar to DTC, CRW shows a drop consistent with Phase I studies for LEU+ and ATF. For PWR multi-assembly models, a drop of around 19% was observed for both fuel types. CBW for BWR multi-assembly models cannot be calculated using the Polaris supercell approach because ATF assemblies require special adjustments due to the significant difference in fuel weight with respect to shuffled-out LEU fuel. However, full-core analysis demonstrated similar reductions to those observed in Phase I studies.

5. During this analysis, inconsistencies between the PARCs and Polaris k_{eff} values at BOC were observed. These inconsistencies were found to originate from the PARCS Xe and Sm models; these issues were noted and communicated to the PARCS development team as future development needs.

REFERENCES

[1] "SCALE Code System," Oak Ridge National Laboratory, Oak Ridge, TN, Tech. Rep. ORNL/TM-2005/39, Version 6.2.4, Apr. 2020. [Online]. Available: https://www.ornl.gov/file/scale-62-manual/display.

[2] M. A. Jessee, W. A. Wieselquist, T. M. Evans, S. P. Hamilton, J. J. Jarrell, K. S. Kim, J. P. Lefebvre, R. A. Lefebvre, U. Mertyurek, A. B. Thompson, and M. L. Williams, "POLARIS: A New Two-Dimensional Lattice Physics Analysis Capability for the SCALE Code System," in *Proceedings of PHYSOR 2014*, Sep. 2014. [Online]. Available: https://www.osti.gov/biblio/1185407.

[3] T. Downar, Y. Xu, T. Kozlowski, and D. Carlson, "PARCS v3.0 US NRC Core Neutronics Simulator User Manual," University of Michigan, Ann Arbor, MI, Tech. Rep. UM-NERS-09-0001, May 2010. [Online]. Available: https://www.nrc.gov/docs/ML1016/ML101610098.pdf.

[4] G. L. Holloway, J. E. Fawks, and B. W. Crawford, "Core Design and Operating Data for Cycles 2 and 3 of Hatch 1," Electric Power Research Institute (EPRI), Tech. Rep. EPRI-2106, Feb. 1984. [Online]. Available: https://www.osti.gov/biblio/5160422.

[5] J. Leppänen, M. Pusa, T. Viitanen, V. Valtavirta, and T. Kaltiaisenaho, "The serpent monte carlo code: Status, development and applications in 2013," *Annals of Nuclear Energy*, vol. 82, pp. 142–150, 2015, ISSN: 0306-4549. DOI: 10.1016/j.anucene.2014.08.024. [Online]. Available: https://www.sciencedirect.com/science/article/pii/S0306454914004095.

[6] R. M. Cumberland, R. T. Sweet, U. Mertyurek, R. Hall, and W. A. Wieselquist, "Isotopic and Fuel Lattice Parameter Trends in Extended Enrichment and Higher Burnup LWR Fuel, Volume II: BWR," Oak Ridge National Laboratory, Oak Ridge, TN, Tech. Rep. ORNL/TM-2020/1835, Mar. 2021. DOI: 10.2172/1782042. [Online]. Available: https://www.osti.gov/biblio/1782042.

[7] R. Hall, R. Cumberland, R. Sweet, and W. A. Wieselquist, "Isotopic and Fuel Lattice Parameter Trends in Extended Enrichment and Higher Burnup LWR Fuel Vol. I: PWR fuel," Oak Ridge National Laboratory, Oak Ridge, TN, Tech. Rep. ORNL/TM-2020/1833, Feb. 2021. DOI: 10.2172/1779134. [Online]. Available: https://www.osti.gov/biblio/1779134.

[8] R. Hall, R. Sweet, R. Belles, and W. A. Wieselquist, "Extended Enrichment Accident Tolerant LWR Fuel Isotopic and Lattice Parameter Trends," Oak Ridge National Laboratory, Oak Ridge, TN, Tech. Rep. ORNL/TM-2021/1961, Mar. 2021. DOI: 10.2172/1783010. [Online]. Available: https://www.osti.gov/biblio/1783010.

[9] "Westinghouse Advanced Doped Pellet Technology (ADOPT) Fuel," Westinghouse Electric Company, Tech. Rep. WCAP-18482-NP, 2020.

[10] S. Cole, C. Delafoy, R. Graebert, P. Louf, and N. Teboul, "AREVA optimized fuel rods for LWRs," in *Transactions of Top Fuel Reactor Fuel Performance 2012*, Manchester, UK, Sep. 2012.

[11] Y. Lin, R. Fawcett, S. Desilva, D. Lutz, M. Yilmaz, P. Davis, R. Rand, P. Cantonwine, R. Rebak, R. Dunavant, and N. Satterlee, "Path Towards Industrialization of Enhanced Accident Tolerant Fuel," in *Proceedings of TOPFUEL 2018*, A0141, Prague, Czech Republic, Sep. 2018.

[12] F. Franceschini, E. Lahoda, J. King, B. Oelrich, and S. Ray, "Transition cycle analysis for optimum ATF implementation in current PWRs," in *Proceedings of TOPFUEL 2018*, A0001, Prague, Czech Republic, Sep. 2018.

[13] J. W. Bae, U. Mertyurek, and M. Asgari, "LEU+ BWR Lattice Design Optimization of Using SCALE/Polaris," in *PHYSOR 2022: International Conference on Physics of Reactors*, May 2022. DOI: 10.13182/PHYSOR22-37710. [Online]. Available: https://www.osti.gov/biblio/1885365.

[14] ——, "Light Water Reactor LEU+ Lattice Optimization," Oak Ridge National Laboratory, Oak Ridge, TN, Tech. Rep. ORNL/TM-2021/2366, Aug. 2022. DOI: 10.2172/1885360. [Online]. Available: https://www.osti.gov/biblio/1885360.

[15] A. Ward, Y. Xu, and T. Downar, "Code for generating the PARCS cross section interface file PMAXS," no. GenPMAXS-v6.3 Release, 2020.

[16] N. H. Larsen and J. G. Goudey, "Core design and operating data for Cycle 1 of Hatch 1," Electric Power Research Institute (EPRI), Tech. Rep. EPRI-562, 1979.

[17] N. S. Folk and W. R. Cobb, "Core performance benchmarking. Edwin I. Hatch Nuclear Plant Unit 1, Cycle 1. Final report," Electric Power Research Institute (EPRI), Tech. Rep. EPRI-1235, Nov. 1979. DOI: 10.2172/5577781. [Online]. Available: https://www.osti.gov/servlets/purl/5577781.

[18] U. Mertyurek and W. A. Wieselquist, "Assessment of Core Physics Characteristics of Extended Enrichment and Higher Burnup LWR Fuels using the Polaris/PARCS Two-Step Approach Vol. II: BWR Fuel," Oak Ridge National Laboratory, Oak Ridge, TN, Tech. Rep. ORNL/TM-2021/1961, 2022.

APPENDIX A. TESTING PROCEDURE FOR PIN POWERS IN A NON-UNIFORM LATTICE GEOMETRY

APPENDIX A. TESTING PROCEDURE FOR PIN POWERS IN A NON-UNIFORM LATTICE GEOMETRY

A.1 TEST PROBLEM

The purpose of this appendix is to describe the testing procedure used to verify the pin power calculation behavior for Polaris as compared to an equivalent lattice physics problem using TRITON/NEWT. For this problem, a 2×2 pin geometry was used consisting of three "nominal" pins and one enlarged pin, wherein the pin radius is increased by 0.0275 cm while the total clad thickness is reduced by the same dimension (thus preserving the outer clad radius and gap thickness). The dimensions for the nominal fuel and enlarged pin are presented in Table 21; this is further illustrated as Figure 39. In order to simplify the comparison, the cladding and fuel material is uniform across all pins (i.e., Zircaloy-2 and 3.9 $^{w}/_{o}$ ^{235}U UO_2); as such, the only substantial difference between the pins is in the size of the fuel region (and thus the fuel mass) itself.

Table 21. Pin dimensions used for 2×2 lattice test of non-uniform pin dimensions

	Nominal	Enlarged
Fuel radius (cm)	0.438	0.4655
Clad inner radius (cm)	0.447	0.4745
Clad outer radius (cm)	0.513	0.513

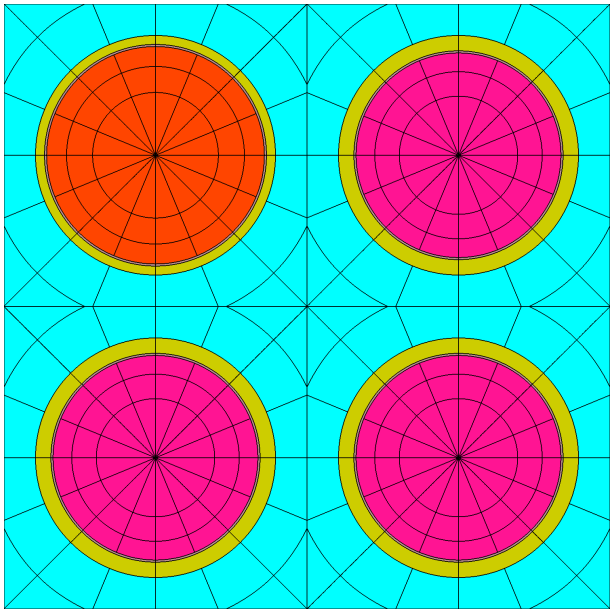

Figure 39. 2×2 lattice with nominal pins and one enlarged pin (NW corner) used for testing power normalization against TRITON/NEWT.

A.2 TEST RESULTS

The results for the enlarged pin test are shown in Table 22.

Table 22. Relative pin powers and pin power differences for 2x2 non-uniform pin lattice test.

TRITON/NEWT		Polaris		Difference (%)	
1.0846	0.9708	1.0024	1.0056	-7.58	+3.58
0.9708	0.9739	0.9911	1.0021	+2.09	+2.90

A.3 TEST INPUTS

A.3.1 POLARIS 56-GROUP TEST INPUT

```
=polaris
title "Thick pin test"
lib "xn56v7.1"
%
sys BWR
geom FuelNode : ASSM 2 1.2954
channel COOL
opt CRITSPEC Mode='none'
% Standard ZIRC2 cladding
mat CLAD.2 : ZIRC2  temp=560
mat FUEL.5 : uox39  temp=950 dens=10.4
comp uox39 UOX 3.9
mat FUEL.6 : uox39  temp=950 dens=10.4
mat GAP.1 : he_GAP  temp=560
    comp  he_GAP : CONC
          2003=1.50456E-11
          2004=1.50456E-05
mat COOL.1 : h2o_mod  temp=560
    comp  h2o_mod : CONC
          1001=3.06145E-02
          8016=1.53073E-02

pin  L1  :  0.438  0.447  0.513 :  FUEL.5   GAP.1  CLAD.2
pin  L2  :  0.4655 0.4745  0.513 : FUEL.6   GAP.1  CLAD.2
pinmap
 L2  L1
 L1  L1

mesh COOL   : nx=9 ny=9 ns=16 nr=2
mesh COOL.2 : nx=9 ny=9 ns=16 nr=4
mesh MOD    : nf=4 nd=5 nx=10 ny=10 ns=16 nr=4
mesh FUEL   : nr=3 ns=16
mesh TUBE   : ns=16
end
```

A.3.2 TRITON/NEWT 56-GROUP TEST INPUT

```
=t-newt
pwr ce 14x14, 1/4 assembly model
v7-56
read composition
h-1   4 0   3.06145E-02 560 end
o-16   4 0  1.53073E-02 560 end
h-1   44 0   3.06145E-02 560 end
o-16  44 0  1.53073E-02 560 end
uo2    1 den=10.4 1  950
                    92235 3.9
                    92238 96.1   end
uo2   11 den=10.4 1  950
                    92235 3.9
                    92238 96.1   end
zirc2  3 1 560   end
zirc2 33 1 560   end
n      2 den=0.0000125 1 560 end
n     22 den=0.0000125 1 560 end
end composition
read celldata
  latticecell squarepitch fuelr=0.4655 1 gapr=0.4745 2
     cladr=0.513 3 hpitch=0.6477 4 end
  latticecell squarepitch fuelr=0.438 11 gapr=0.447 22
     cladr=0.513 33 hpitch=0.6477 44 end
end celldata
read model
read parameter
 drawit=no cmfd=yes xycmfd=2 sn=16 echo=yes
end parameter
read materials
  mix=1  pn=1 com='fuel fat'  end
  mix=11 pn=1 com='fuel'  end
  mix=2  pn=0 com='gap'  end
  mix=3  pn=0 com='clad'  end
  mix=4  pn=2 com='mod'  end
end materials
read geometry
unit 1
com="fat fuel pin"
 cylinder 1    0.4655
 cylinder 2    0.4745
 cylinder 3    0.513
 cuboid 4   0.6477  -0.6477   0.6477  -0.6477
 media 1 1 1
 media 2 1 2 -1
 media 3 1 3 -2
```

```
 media 4 1 4 -3
 boundary 4 4 4
unit 2
com="fuel pin"
 cylinder 1    0.438
 cylinder 2    0.447
 cylinder 3    0.513
 cuboid 4   0.6477  -0.6477   0.6477  -0.6477
 media 11 1 1
 media 2 1 2 -1
 media 3 1 3 -2
 media 4 1 4 -3
 boundary 4 4 4
global unit 10
com="1/4 assembly"
 cuboid 1   1.2954   -1.2954   1.2954  -1.2954
 array 1 1  place 1 1  -0.6477  -0.6477
 media 4 1 1
 boundary 1 8 8
end geometry
read array
ara=1 nux=2 nuy=2  pinpow=yes
 fill
    1    2
    2    2      end fill
end array
end model
end
```